SEMMELWEIS EGYETEM

DOKTORI ISKOLA

Ph.D. értekezések

3083.

BEDICS GÁBOR

Onkológia
című program

Programvezető: Dr. Bödör Csaba, egyetemi tanár

Témavezető: Dr. Alpár Donát, tudományos főmunkatárs

GENOMIC PROFILING OF PEDIATRIC MALIGNANT HEMATOPOIETIC AND LYMPHOID DISEASES BY NEXT-GENERATION SEQUENCING-BASED METHODS AND BIOINFORMATIC APPROACHES

PhD thesis

Gábor Bedics

Pathological Sciences Doctoral School

Semmelweis University

Supervisor:	Donát Alpár, PhD
Official reviewers:	Gergely Varga, MD, PhD
	András Bors, PhD

Head of the Complex Examination Committee:	Monika Csóka, MD, PhD
Members of the Complex Examination Committee:	Gergely Kriván, MD, PhD
	Gábor Turu, MD, PhD

Budapest

2024

TABLE OF CONTENTS

LIST OF ABBREVIATIONS

1000Genomes	1000 Genomes Project
AA	Amino Acid
ABL1	Abelson Tyrosine-Protein Kinase 1
ADP	Adenosine Diphosphate
ALK	Anaplastic Lymphoma Receptor Tyrosine Kinase
ALL	Acute Lymphoblastic Leukemia
ARAF	A-Raf Proto-Oncogene Serine/Threonine Kinase
ARF	Adenosine Diphosphate Ribosylation Factor
B-ALL	B-Cell Acute Lymphoblastic Leukemia
BAM	Binary Alignment Map
BCR	Breakpoint Cluster Region
BRAF	B-Raf Proto-Oncogene Serine/Threonine Kinase
BTG1	B-Cell Translocation Gene 1 Protein
BTLA	B- And T-Lymphocyte Attenuator
CASP8AP2	Caspase 8 Associated Protein 2
CD200	Cluster of Differentiation 200
CDKN2A/B	Cyclin Dependent Kinase Inhibitor 2A/B
cDNA	Complementary Deoxyribonucleic Acid
Chr	Chromosome
CNA	Copy Number Aberration
CNS	Central Nervous System
COSMIC	Catalogue of Somatic Mutations in Cancer
CRAFT	CNV Robust Analysis For Tumors
CYTO	Cytogenetic
dbSNP	Single Nucleotide Polymorphism Database
digitalMLPA	Digital Multiplex Ligation-dependent Probe Amplification
DNA	Deoxyribonucleic Acid
DUX4	Double Homeobox 4
EFS	Event-Free Survival
EMA	European Medicines Agency
ETP	Etoposide

ETV6	ETS Variant Transcription Factor 6
FDA	Food and Drug Administration
FFPE	Formalin-Fixed Paraffin-Embedded
FISH	Fluorescence In Situ Hybridization
GAP	Guanosine Triphosphatase Activating Protein
GENCODE	Genomic Encyclopedia of DNA Elements
GIT2	G Protein-Coupled Receptor Kinase-Interactor 2
GnomAD	Genome Aggregation Database
GR	Good-Risk
GTG	G-bands After Trypsin and Giemsa
GTP	Guanosine Triphosphate
HHD	High Hyperdiploidy
HR	High-Risk
i.th.	Intrathecal
i.v.	Intravenous
iAMP21	Intrachromosomal Amplification of Chromosome 21
IC-BFM	Intercontinental Berlin-Frankfurt-Münster Study Group
IFO	Ifosfamide
IHC	Immunohistochemistry
IKZF1	IKAROS Family Zinc Finger 1
IKZF1^{del}	IKAROS Family Zinc Finger 1 deletion
IKZF1^{plus}	IKAROS Family Zinc Finger 1 plus
InDel	Insertion-Deletion
IR	Intermediate-Risk
KMT2A	Lysine (K) Methyltransferase 2A
KRAS	Kirsten Rat Sarcoma Viral Oncogene Homolog
MAP2K1	Mitogen-Activated Protein Kinase Kinase 1
MAPK	Mitogen-Activated Protein Kinase
MLLT3	Myeloid/Lymphoid or Mixed-Lineage Leukemia Translocated to Chromosome 3 Protein
MLPA	Multiplex Ligation-dependent Probe Amplification
MR	Medium-Risk

MRD	Measurable Residual Disease
MRI	Magnetic Resonance Imaging
MSI	Microsatellite Instability
MTX	Methotrexate
NCBI	National Center for Biotechnology Information
NGS	Next-Generation Sequencing
NRAS	Neuroblastoma RAS Viral Oncogene Homolog
NSCLC	Non-Small Cell Lung Cancer
NUP214	Nucleoporin 214
OS	Overall Survival
PAR1	Pseudoautosomal Region 1
PAX5	Paired Box 5
PBX1	Pre-B-Cell Leukemia Homeobox 1
PCR	Polymerase Chain Reaction
PDGFRB	Platelet Derived Growth Factor Receptor Beta
PR	Poor-Risk
pred.	Prednisolone
QCI	QIAGEN Clinical Insight
RB1	Retinoblastoma 1
RefSeq	National Center for Biotechnology Information Reference Sequence Database
RNA	Ribonucleic Acid
ROS1	Receptor Tyrosine Kinase C-Ros Oncogene 1
RUNX1	Runt-Related Transcription Factor 1
SNV	Single Nucleotide Variant
SR	Standard-Risk
STAR	Spliced Transcripts Alignment to a Reference
t-SNE	t-Distributed Stochastic Neighbor Embedding
T1	Longitudinal Relaxation Time
TARGET	Therapeutically Applicable Research to Generate Effective Treatments
TBL1XR1	Transducin Beta Like 1 X-Linked Receptor 1

TCF3	Transcription Factor 3
TMB	Tumor Mutational Burden
TP53	Tumor Protein P53
UMI	Unique Molecular Identifier
VBL	Vinblastine
VPREB1	V-Set Pre-B Cell Surrogate Light Chain 1
W	Watt
ZNF384	Zinc Finger Protein 384

1. Introduction

1.1. Epidemiology and distribution of pediatric malignant diseases with special focus on hematopoietic and lymphoid tumors

Cancer is a leading cause of mortality among children aged 1 to 14 years in Western countries, surpassed only by accidents; and it is the fourth most common cause of death among adolescents, aged 15-19 years (1). According to an estimation by the American Cancer Society, approximately 9,620 young children and 5,290 adolescents will be diagnosed with cancer, and 1,040 young children and 550 adolescents will die from the disease in the United States in 2024 (1). Standardized incidence of pediatric (aged 0-18 years) malignant diseases is approximately 150 per million in Hungary, with around 280 novel diagnoses per year (2).

Malignant diseases of hematopoietic and lymphoid tissues (leukemias, myeloproliferative-, and myelodysplastic neoplasms, lymphomas as well as reticuloendothelial neoplasms) are responsible for 40% of all pediatric malignancies among young children and for one third of malignant diseases in adolescents. These diseases are followed in incidence by brain and other nervous system tumors accounting for one third of all malignancies among young children and for 25% of the cases in adolescence. The remaining cancer cases include various soft tissue tumors, renal- and hepatic neoplasms, melanomas and other rare entities both among young children and adolescents (Figure 1) (1).

Regarding hematopoietic and lymphoid neoplasms, the most frequent malignant entity of childhood is acute lymphoblastic leukemia, followed by Non-Hodgkin lymphomas, acute myeloid leukemia, Hodgkin lymphoma and other malignant hematological diseases (1). In contrast to adult hematopoietic and lymphoid disorders, pediatric malignancies are more commonly characterized by high-grade biological features and include entities specific for childhood, e.g.: pediatric-type follicular lymphoma and pediatric nodal marginal zone lymphoma (3-5). On the other hand, some frequent entities of adulthood, for example chronic lymphocytic leukemia, occur extreme rarely among children (6).

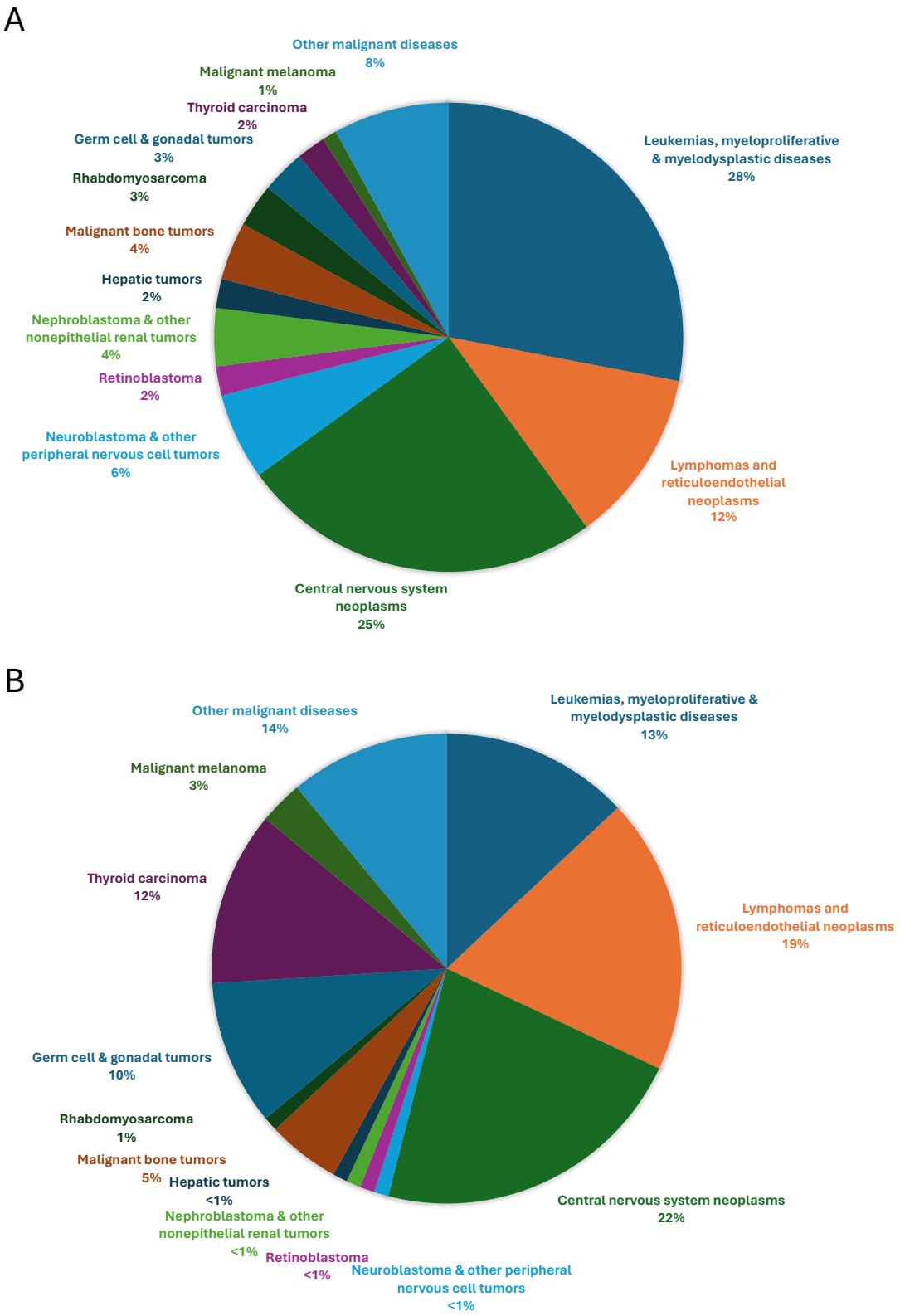

Figure 1. Distribution of pediatric malignant diseases. Recent distribution of pediatric cancer types among (A) young children (birth to 14 years) and (B) adolescents (15 - 19 years) according to the American Cancer Society (1).

1.2. Pediatric B-cell precursor acute lymphoblastic leukemia

Acute lymphoblastic leukemia (ALL), the most common malignant disease of childhood accounts for 80% of all pediatric leukemia cases and displays B-cell precursor phenotype (B-ALL) in approximately 85% of the patients (7).

Due to the application of multiagent chemotherapy regimens and stratification of treatment intensity according to (*i*) the clinical features of the patient, (*ii*) biological characteristics of the leukemic blasts, and (*iii*) early response to treatment, all of which are predictive for the event-free survival, prognosis of pediatric ALL improved progressively over the last five decades (Figure 2). Although the overall survival (OS) of B-ALL exceeds 90% in Westerns countries, integration of novel molecular genetic data and advancements in biotechnology may further facilitate the improvement of patient survival (8).

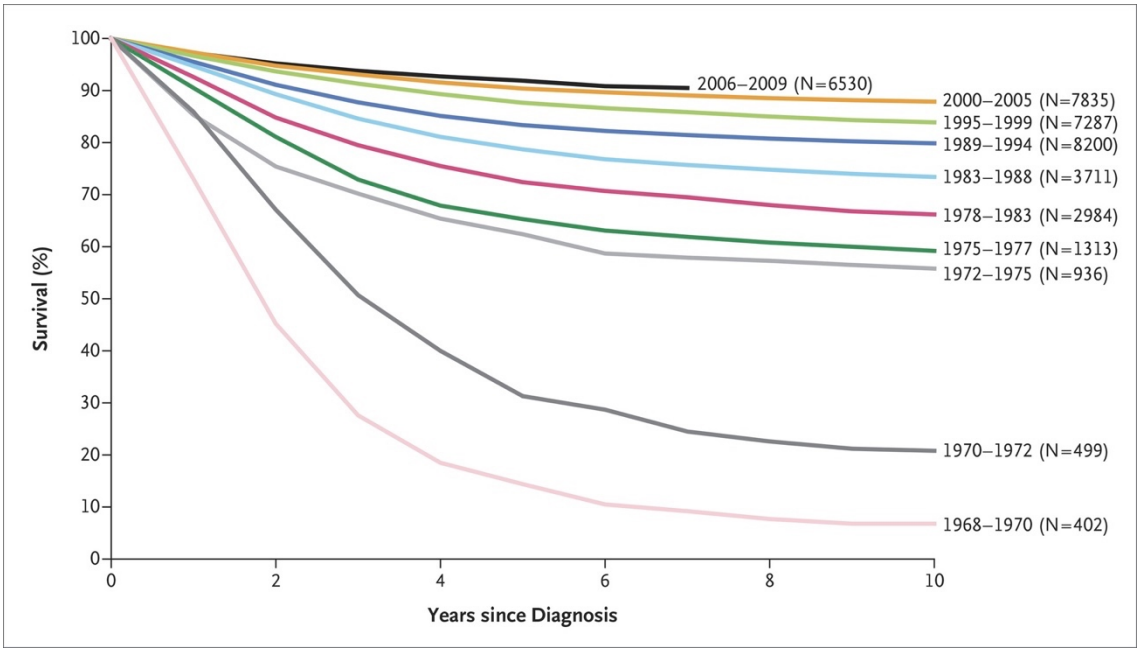

Figure 2. Improvement of overall survival in pediatric ALL over the last decades. Overall survival among children with acute lymphoblastic leukemia enrolled in Children's Cancer Group and Children's Oncology Group clinical trials, 1968-2009. Adapted from Hunger and Mullighan, Acute Lymphoblastic Leukemia in Children, NEJM, 2015 (8).

Pediatric ALL develops in multiple steps, with the initiating genomic lesion emerging *in utero*, as demonstrated in major genetic subtypes, followed by the rise of secondary aberrations required for the clinical manifestation of the disease (9-12).

The most recent large-scale genomic study, summarizing whole genome, exome and transcriptome sequencing data of 2,754 patients with pediatric ALL, determined a median of 4 putative somatic driver genetic variations per sample, despite a generally low tumor mutational burden (TMB) and identified 376 putative driver genes with various prevalence in pediatric ALL (12). In this study, Brady et al. classified B-ALL cases into 23 different subgroups enabling a refined molecular subtyping (12).

Current classification (5th edition) of the World Health Organization (WHO) includes 13 B-ALL subgroups determined by presence or absence of (*i*) numerical or subchromosomal copy number aberrations (CNAs) (B-ALL with high hyperdiploidy, hypodiploidy and iAMP21), (*ii*) gene rearrangements (e.g.: B-ALL with *ETV6*::*RUNX1*, *BCR*::*ABL1* or *KMT2A* fusions), or (*iii*) gene expression profiles (e.g.: B-ALL with *BCR*::*ABL1*-like signature) (13, 14). This WHO classification also describes novel subtypes, defined by (*i*) a rare, but clinically crucial gene fusion (*TFC3::HLF*), which is targetable with approved therapeutic approaches such as the CD19-directed bispecific antibody blinatumomab and the BCL2-inhibitor venetoclax (15-17), and (*ii*) B-ALL with *ETV6*::*RUNX1*-like features subgroup, which is determined by similarity in gene expression to the subgroup characterized by *ETV6*::*RUNX1* gene fusion. This latter subgroup bears prognostic relevance and may enhance risk assessment and patient stratification (Table 1.) (18).

Besides these advances in WHO classification, there are additional emerging biomarkers, e.g. *DUX4* translocation, *PAX5* alterations and *ZNF384* fusions, which currently do not define official subgroups but have associated prognostic/predictive power and recurrently contribute to the heterogeneous genetic landscape of pediatric B-ALL (Figure 3.) (18-20).

Table 1. Comparison of the fifth and fourth editions of WHO classifications of precursor B-cell neoplasms. Comparison of the two recent editions was adapted from Alaggio et al.: The 5th edition of the World Health Organization Classification of Haematolymphoid Tumours: Lymphoid Neoplasms, Leukemia, 2022 (14).

WHO Classification, 5th edition	**WHO Classification, revised 4th edition**
B-ALL, NOS	(Same)
B-ALL with high hyperdiploidy	B-ALL with hyperdiploidy
B-ALL with hypodiploidy	(Same)
B-ALL with iAMP21	(Same)
B-ALL with *BCR*::*ABL1* fusion	B-ALL with t(9;22)(q34;q11.2); *BCR-ABL1*
B-ALL with *BCR*::*ABL1*-like features	B-ALL, *BCR-ABL1*-like
B-ALL with *KMT2A* rearrangement	B-ALL with t(v;11q23.3); *KMT2A*-rearranged
B-ALL with *ETV6*::*RUNX1* fusion	B-ALL with t(12;21)(p13.2;q22.1); *ETV6-RUNX1*
B-ALL with *ETV6*::*RUNX1*-like features	*Not defined*
B-ALL with *TCF3*::*PBX1* fusion	B-ALL with t(1;19)(q23;p13.3); *TCF3-PBX1*
B-ALL with *IGH*::*IL3 fusion*	B-ALL with t(5;14)(q31.1;q32.1); *IGH*/*IL3*
B-ALL with *TCF3*::*HLF* fusion	*Not defined*
B-ALL with other defined genetic abnormalities	(Same)

Copy number aberrations such as whole chromosome gains and losses as well as subchromosomal imbalances recurrently occur as primary or secondary alterations, substantially contributing to the heterogeneous genomic landscape of ALL (21-24).

The vast majority of numerical chromosome aberrations emerge in the high-hyperdiploid subgroup which accounts for 25-30% of pediatric B-ALL patients, with the leukemic blasts in this subgroup bearing non-random gains of specific chromosomes conferring a modal chromosome number of 51-67 (25, 26). Subchromosomal CNAs recurrently affect

genes involved in cell cycle control, tumor suppression, lymphoid cell development and B-cell differentiation (21).

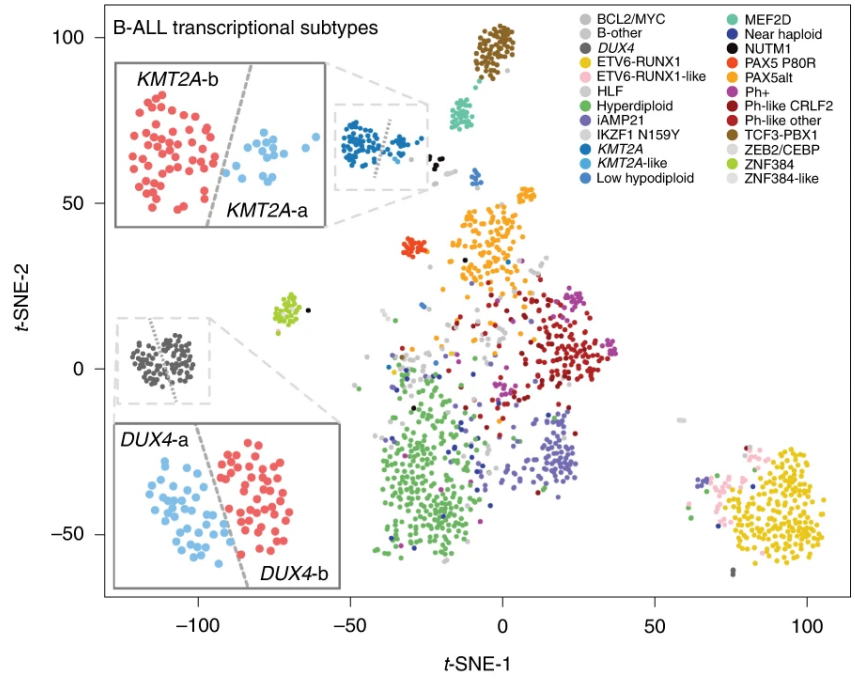

Figure 3. Heterogeneous molecular landscape of pediatric B-ALL according to the most recent large-scale study published by Brady et al. Gene expression profiles of various subgroups are displayed on two-dimensional t-distributed stochastic neighbor embedding (t-SNE) plot (12).

A wide range of methods is available for screening CNAs in pediatric ALL, including karyotyping, fluorescence *in situ* hybridization (FISH), DNA index measurement, multiplex ligation-dependent probe amplification (MLPA), cytogenomics, optical genome mapping as well as various array- and next-generation sequencing (NGS) based approaches (11, 21, 27-29). DigitalMLPA is a recently developed technique which combines MLPA with NGS readout providing a high-throughput, scalable, highly rationalized but still comprehensive means to interrogate recurrently affected genomic loci with a short turn-around time as previously demonstrated by our group and others (30-32).

Several studies investigated the clinical significance of CNAs in pediatric ALL and identified a range of prognostic biomarkers based on modal chromosome number (33-

36), specific trisomies (34, 35, 37, 38), double or triple trisomies (34-36, 39, 40), simultaneous presence and absence of various trisomies (41), loss or gain/amplification of key driver genes (42, 43), as well as specific alteration patterns of predefined gene sets (44). These observations facilitated the widespread implementation of CNA screening in the diagnostics of pediatric ALL, with an aim to support patient stratification and potentially aid therapy selection.

Integrative efforts have led to the establishment of complex classifiers enabling the assignment of patients to distinct prognostic subgroups based on cytogenetic and molecular genetic markers (32, 44-46). Shortcomings of current genetic classifiers are the relatively low number and limited combinations of aberrations used as criteria for decision making. Assignment of individual patients is typically restricted to a couple of specific genomic patterns; for example, trisomy of chromosomes 17 and/or 18 without extra copies of chromosomes 5 and 20; isolated *IKZF1* deletion; isolated deletion of *ETV6*, *PAX5* or *BTG1*; co-occurrence of *IKZF1* deletion with deletion of *CDKN2A*, *CDKN2B*, *PAX5* or PAR1 in the absence of *ERG* deletion; *ETV6* deletion with single deletion of *BTG1*, *CDKN2A/B* or *PAX5*, with all other uncategorizable patients being classified in the same non-specific, collective subgroup.

1.3. Histiocytic neoplasms

Histiocytic and dendritic cell neoplasms are rare tumors originating from common myeloid progenitors and showing differentiation towards cells of the mononuclear phagocyte system, comprising monocytes, macrophages and dendritic cells (13, 47). Histiocytic neoplasms display macrophage differentiation and include histiocytic sarcoma, Rosai-Dorfman-Destombes disease, ALK-positive histiocytosis, Erdheim-Chester disease, and juvenile xanthogranuloma; although, this last entity has also been suggested to originate from dermal/interstitial dendritic cells (Table 2) (13). Diagnostics of these entities can be challenging due to the highly overlapping histopathological and molecular features (13, 47, 48).

Table 2. Entities of histiocytic neoplasms according to the WHO classification of haematolymphoid tumours 5th edition (13).

Histiocytic neoplasms
Juvenile xanthogranuloma
Erdheim-Chester disease
Rosai-Dorfman-Destombes disease
ALK-positive histiocytosis
Histiocytic sarcoma

Histiocytic neoplasms frequently harbor mutations in genes of the mitogen-activated protein kinase (MAPK) pathway, such as *BRAF, NRAS*, *KRAS, ARAF* and *MAP2K1,* however with variable frequencies, which suggests a unifying genetic landscape of these diseases (Figure 4) (47). The most recently described, predominantly pediatric ALK-positive histiocytosis (49, 50) displays convergence on the MAPK pathway, which is one of the signaling pathways enhanced by ALK activation (Figure 4) (51, 52).

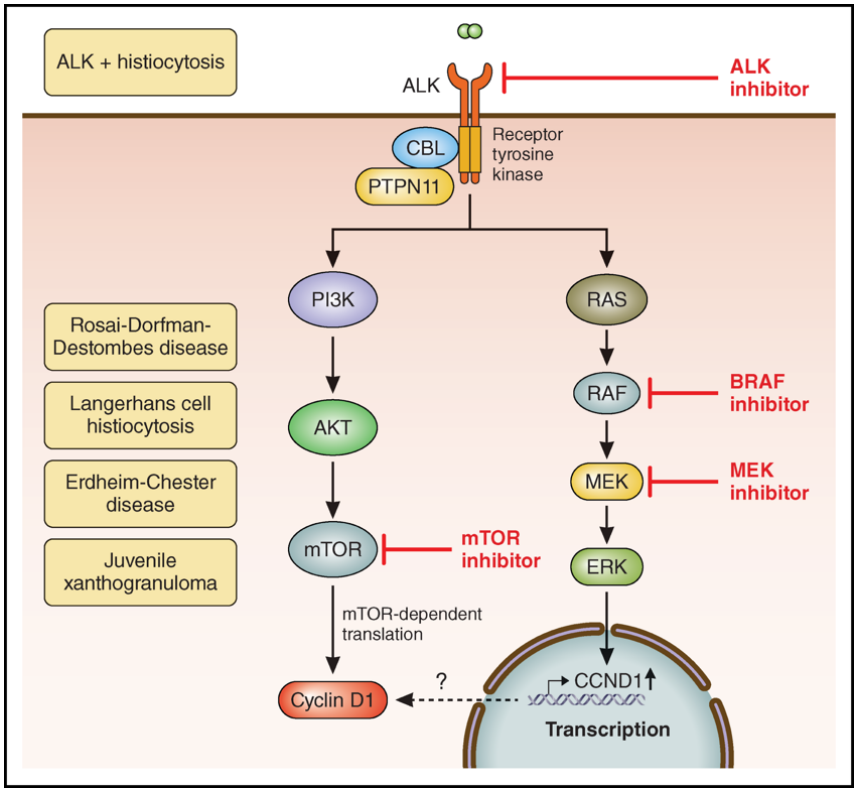

↑**Figure 4: Schematic figure of signal transduction molecules and targeted therapeutic approaches in various histiocytic neoplasms.** Driver molecular alterations of histiocytic neoplasms typically converge on common signaling pathways. The presence of specific inhibitors that can target components of the pathway has led to advances in clinical management and improved prognosis of neoplasms with histiocytic and dendritic cell lineages. Adapted from Kemps et al., ALK-positive histiocytosis: a new clinicopathological spectrum highlighting neurological involvement and responses to ALK inhibition. Blood. 2022 (52).

These genetic features are exploitable by molecularly targeted therapeutic approaches, such as BRAF and MEK inhibitions, which have the potential to effectively target components of the activated signaling pathway, offering durable responses for the patients (Figure 4) (52-56).

2. OBJECTIVES

During my PhD research, we aimed:

1. To perform comprehensive screening for disease-relevant CNAs in a cohort of Hungarian pediatric patients diagnosed with B-ALL using digitalMLPA, a novel next-generation sequencing-based molecular technique.
2. To analyze co-segregating variants and WHO subgroups, displaying co-occurrence or mutually exclusive appearance in pediatric B-ALL.
3. To scrutinize whole chromosome gains individually and in combinations to identify specific patterns associated with favorable outcome among B-ALL patients with high-hyperdiploid karyotype as revealed or confirmed by digitalMLPA.
4. To analyze *IKZF1* status at exon level (provided by digitalMLPA method) and combine *IKZF1* status (*IKZF1*^{normal}, *IKZF1*^{del} and *IKZF1*^{plus}) with cytogenetic classes, thus creating a cytogenetics aware interpretation of *IKZF1* imbalance in pediatric B-ALL.
5. To introduce a conceptually novel patient classification approach, which assigns B-ALL patients to prognostic subgroups based on highly individualized cumulative scores reflecting the weighted impact of all relevant aberrations detected in a particular patient.
6. To validate our findings regarding the detected CNAs and the conceptually novel patient classification approach for pediatric B-ALL on a large-scale independent validation cohort with *in-silico* approach.
7. To perform comprehensive genetic characterization and relevant independent validation analyses on the first *ROS1* translocated histiocytic neoplasm sample.
8. To assess clinicopathological features of a molecularly targeted therapeutic attempt with ROS1-inhibitor entrectinib with off-label indication on the first patient diagnosed with *ROS1* translocated histiocytic neoplasm.

3. METHODS

3.1. Comprehensive disease-relevant DNA copy number aberration profiling in pediatric acute lymphoblastic leukemia

3.1.1. Patient samples

In the frame of the Hungarian Pediatric Leukemia Molecular Profiling Program, diagnostic bone marrow samples from 260 patients (male:female ratio: 1.43:1) diagnosed with B-cell precursor ALL at age 1-17 years (median: 5 years) were investigated. Diagnoses were made based on morphological, immunophenotypical and genotypical criteria in the Department of Pathology and Experimental Cancer Research, Semmelweis University, in the Department of Pathology, University of Pécs, or in the Department of Pathology, University of Debrecen between 2003 and 2019 (7, 57, 58). Specimens contained on average 79% (range: 29–99%) leukemic blasts as assessed by flow cytometry.

Baseline genetic characterization of patient samples included DNA index measurement by flow cytometry, karyotyping by GTG-banding, fluorescence *in situ* hybridization for *BCR::ABL1* and *ETV6::RUNX1* fusions, *KMT2A* and *TCF3* rearrangements, and trisomy of chromosomes 4 and 10 using Vysis probes (Abbott Diagnostics, Abbott Park, IL, USA), as well as quantitative PCR tests for *BCR::ABL1* and *ETV6::RUNX1* fusions, and conventional MLPA using the SALSA 202 and 335 probemixes (MRC Holland, Amsterdam, the Netherlands).

Risk assessment and treatment selection were performed according to ALL IC-BFM protocols, such as the ALL IC-BFM 2002 (121 patients, 47%) and ALL IC-BFM 2009 (139 patients, 53%) (59). Standard-risk (SR), medium-risk (MR) and high-risk (HR) groups were represented by 35%, 52% and 13%, as well as by 16%, 65% and 19% of the patients in cohorts treated with ALL IC-BFM 2002 and ALL IC-BFM 2009, respectively. The estimated 5-year event-free survival (EFS) rates were similar in groups of patients treated with different versions of the ALL IC-BFM protocol (ALL IC-BFM 2002: 77.8%, ALL IC-BFM 2009: 81.6%, log-rank test: $p = 0.530$) (Figure 5), therefore, data from all 260 patients were combined. In the entire discovery cohort, 65 (25%), 153 (59%) and 42

(16%) patients were stratified in the SR, MR and HR groups, respectively. Ethical approval (45563-2/2019/EKU) from the Medical Research Council of Hungary and written informed consent from the patients and/or from the parents or guardians were obtained for the study, which was conducted in accordance with the Declaration of Helsinki.

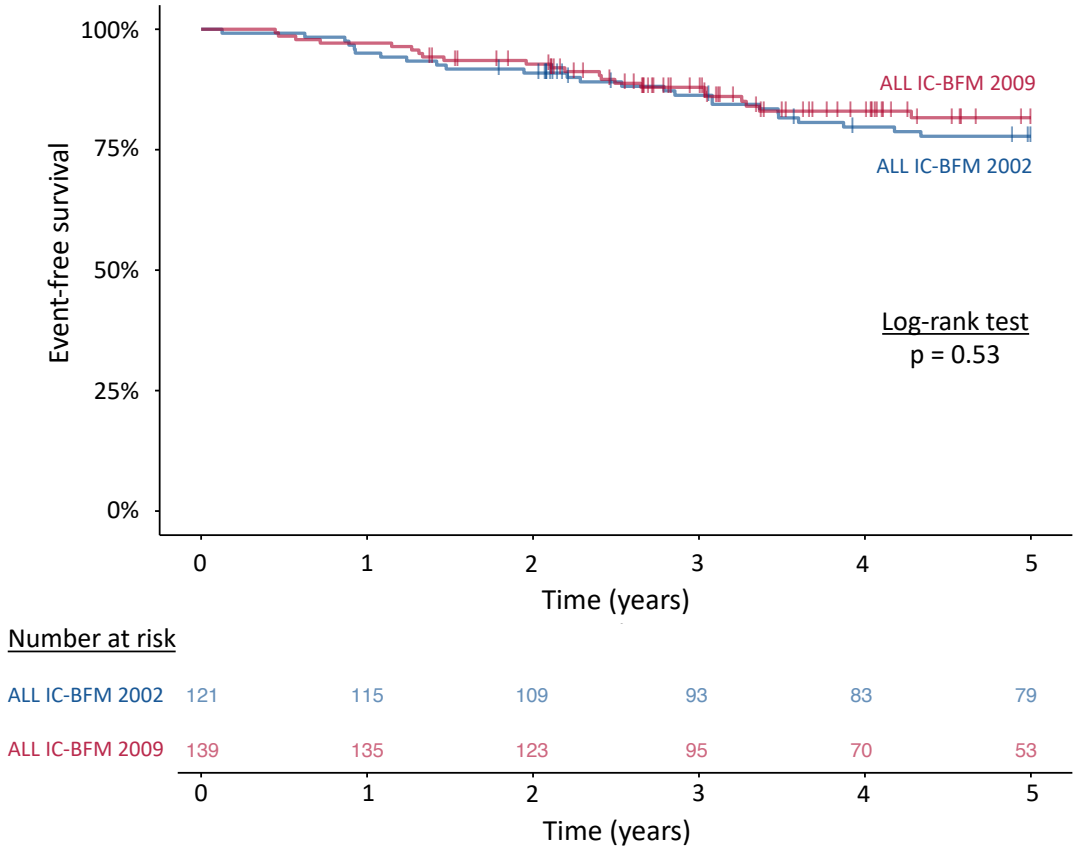

Figure 5. Event-free survival of patients treated with ALL IC-BFM 2002 and ALL IC-BFM 2009 treatment protocols. Estimated 5-year EFS did not show significant difference between the two patient cohorts (77.8% vs. 81.6%, log-rank test: p = 0.530).

3.1.2. digitalMLPA

DigitalMLPA reactions were performed on 40 ng genomic DNA using the D007 ALL probemix (version D007-X2-0516 or D007-X5-0220), which was developed by the MRC Holland and provided to collaborating laboratories for testing and validation. The probemix consisted of (*i*) target probes for regions recurrently altered by copy number aberrations in acute lymphoblastic leukemia; (*ii*) digital karyotyping probes covering all

chromosome arms for detection of gross chromosomal aberrations and serving as reference probes for data normalization, and (*iii*) internal control probes for quality control and sample identification.

DigitalMLPA reactions were carried out according to the previously published protocol (30-32) (Figure 6). Briefly, individual DNA samples were mixed with a unique barcode solution followed by sample denaturation and addition of digitalMLPA probes with digitalMLPA buffer to the reaction mix. Each probe comprised two oligonucleotides with a locus-specific 25–50 bp hybridizing sequence. Probe oligonucleotides binding to a target region were designed to hybridize adjacently; hence, if perfectly bound, could be ligated into a complete probe using the ligase-65 enzyme. Ligated probes were amplified by universal primers compatible with Illumina sequencing platforms. Barcoded, sample-specific PCR products from different reactions were pooled and sequenced on a MiSeq v3 standard flow cell (Illumina, San Diego, CA, USA) using 110 bp or 115 bp single-read chemistry.

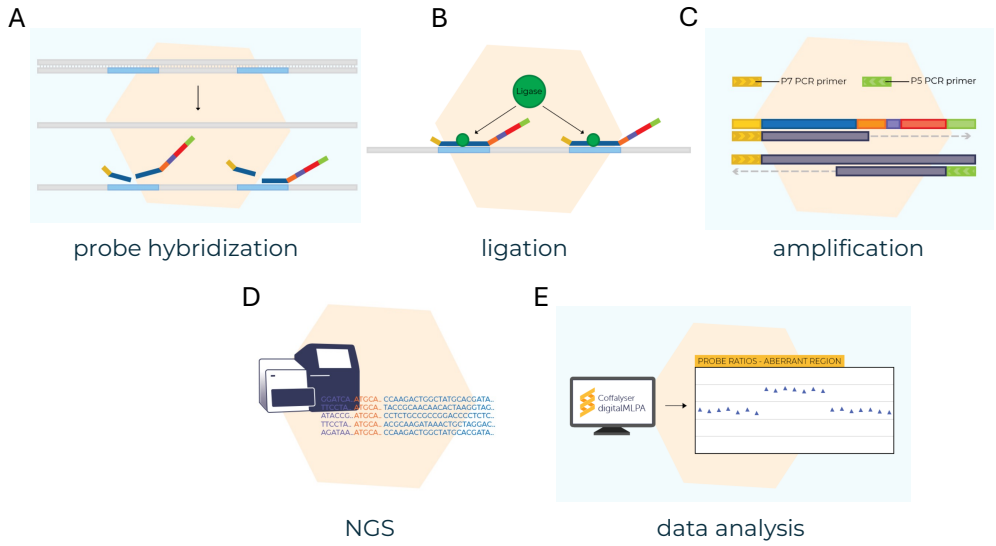

Figure 6. Schematic protocol of digitalMLPA. Probe oligonucleotide pairs hybridize to disease-specific target regions of a denatured DNA sample (A). In case of perfect hybridization, a ligation step connects the probe fragments, creating a set of complete, amplifiable probes (B). Ligated full probes are amplified with PCR (C) and sequenced on Illumina NGS platform (D), with bioinformatic analysis being performed by the Coffalyser digitalMLPA software developed by the vendor (E). Source of figures: www.mrcholland.com

Copy number status at each interrogated locus was determined from the NGS output in two consecutive steps using the Coffalyser digitalMLPA software v.004 (MRC Holland). First, read count corresponding to each probe was normalized by the read counts generated from reference probes hybridizing to copy number stable regions of the same genome. Second, the relative read count calculated for each probe was compared with the matching values of all reference samples. The final probe ratio value (dosage quotient) was around 1.0 if the analyzed region was unaffected by copy number aberration, while an increased or decreased value indicated the presence and level of gain or loss, respectively. Leukemic cell purity as assessed by flow cytometry was also considered at the interpretation of the results. CNAs were reported as being subclonal if multiple consecutive probes had dosage quotients unambiguously falling outside the normal range but without reaching the expected level of monoallelic loss as calculated based on sample purity, and also compared with other altered regions within the same specimen.

3.1.3. Validation cohort - origin and analysis

The independent validation cohort comprised 606 patients included in the Acute Lymphoblastic Leukemia Pilot Phase 1 (phs0000463) or the Expansion Phase 2 (phs000464) studies of the Therapeutically Applicable Research to Generate Effective Treatments - TARGET initiative (https://ocg.cancer.gov/programs/target), and genomically profiled at the St. Jude Children's Research Hospital or at the Baylor College of Medicine using Gene Chip Human Mapping 500 K Array (Affymetrix) or SeqCap EZ Human Exome 2.0 (Nimblegen), respectively. Patients diagnosed with B-ALL at age <18 and having reported EFS values were included, while exclusion criteria comprised Down-syndrome and early toxicity during induction therapy. After reviewing the Affymetrix 500 K Array results downloaded from the TARGET website, CNAs with copy number segments of >2.3 or <0.7 as reported by the St. Jude Children's Research Hospital were considered in our validation analyses. Whole-exome sequencing derived BAM files aligned to the reference genome Human Build 37 (NCBI) were downloaded and CNAs were called by the CNVkit v.0.9.10.dev0 software utilizing a circular binary segmentation method (60-62). Log2 ratio estimates were normalized based on sex of the patients and on reported leukemic cell purity assessed by flow cytometry. Genetic subgroups and 5-

year EFS in the validation cohort and in our in-house discovery cohort are shown in Table 3 and Figure 7.

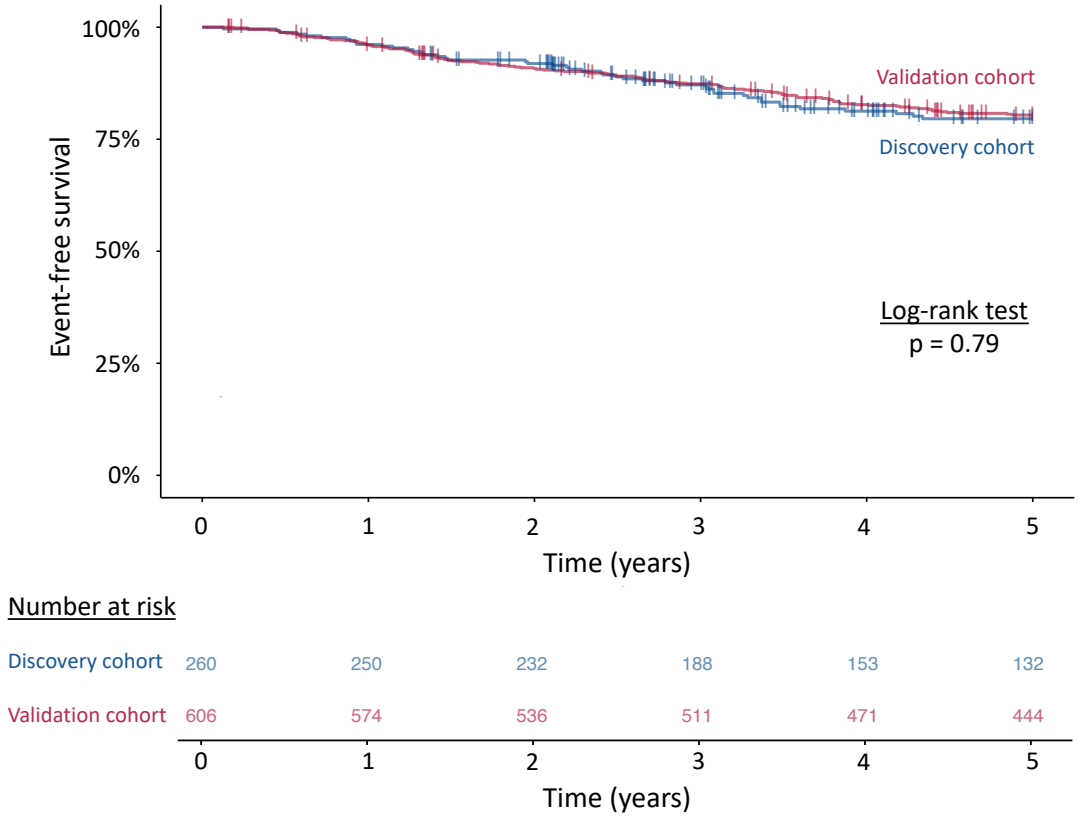

Figure 7: Event-free survival of patients included in our discovery cohort (N = 260) and in the merged TARGET ALL phase 1 pilot and phase 2 expansion cohort (N = 606). Estimated 5-year EFS did not show significant difference between the two patient cohorts (79.6% vs. 80.4%, log-rank test: p = 0.790).

3.1.4. Statistical analysis

Co-segregations of disease-relevant CNAs were analyzed using the "somaticInteraction" function of maftools Bioconductor package (v2.2.10) which performed pairwise Fisher's exact tests and identified significant mutually exclusive or co-occurring events (63). EFS up to 5 years was defined as the time from start of treatment to relapse, second malignancy or disease-related death, excluding early toxicity. Mean follow-up time was 46.6 months (range: 1.5-72.0 months) with at least 24.0 months at patients experiencing no event during the study period. Cox regression models were used for assessing the association of individual genetic aberrations with risk of progression and for building models for

progression prediction. Survival rates were estimated using the Kaplan-Meier method and compared by log-rank tests coupled with Benjamini-Hochberg false discovery rate correction. Statistical analyses were performed using R version 4.1.2 (R Foundation for Statistical Computing, Vienna, Austria, 2021).

Table 3: Distribution of genetic subtypes in our in-house discovery patient cohort and in the merged TARGET ALL phase 1 pilot and phase 2 expansion study cohort used for validation.

Genetic subtype	Discovery cohort ***N = 260***	TARGET ALL P1 & P2 validation cohort ***N = 606***
Hyperdiploidy	31.9%	24.1%
ETV6::RUNX1	26.2%	19.5%
BCR::ABL1	2.3%	1.0%
iAMP21	3.8%	1.8%
KMT2Ar	1.5%	4.1%
TCF3::PBX1	1.2%	6.1%
B-other	34.2%	42.9%

3.2 Discovery and comprehensive genomic profiling of the first histiocytic neoplasm with *ROS1* gene fusion

3.2.1. Clinical symptoms and pathohistological features

A 19-month-old boy presented with visual disturbances as well as vertical nystagmus of the left eye and unstable gait. Magnetic resonance imaging (MRI) revealed multiple subcortical and periventricular white matter lesions also affecting the corpus callosum (Figure 8/A). One single, larger, homogenously contrast-enhancing, dural-based lesion was described in the right cerebellar hemisphere and another intradural extramedullary lesion in the level of the dens axis (Figure 8/A). Outside the central nervous system (CNS), one contrast-enhancing lesion was found above the left lacrimal gland. On the control MRI performed 3 months later, unequivocal increase in the size of previously

detected supratentorial, cerebellar, and spinal lesions was detected. Additionally, one novel contrast-enhancing soft-tissue lesion appeared behind the maxillary sinus (Figure 8/B). Further investigations revealed no systemic involvement. Serological and immunological tests, electro-encephalography as well as cerebrospinal fluid cytology and flow cytometry were negative.

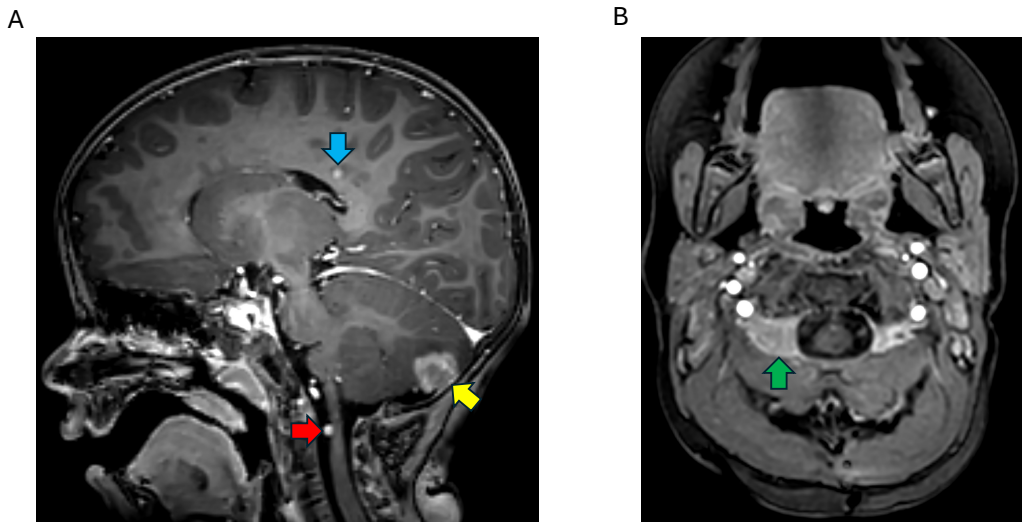

Figure 8: MRI images showing intracranial lesions. MRI (T1-weighted, contrast enhanced) showed (A) multiple white matter (blue arrowhead) as well as single cerebellar (yellow arrowhead) and spinal extramedullary (red arrowhead) lesions, (B) 3 months later, a novel lesion was detected behind the maxillary sinus (green arrowhead).

Biopsy was taken from the cerebellar lesion to explore the nature of the disease. Histology showed a dense infiltrate of neoplastic histiocytes in the cerebellar parenchyma and leptomeningeal surface. Cells contained wide eosinophilic cytoplasm in some areas, while foamy, xanthomatous cells and scattered Touton-type giant cells were observed in others (Figure 9/A,B). Nuclear atypia was mild to moderate and the mitotic activity was inconspicuous. A reactive infiltrate of lymphocytes and eosinophilic granulocytes as well as marked fibrosis were readily detectable (Figure 9/A,B). Tumor cells showed diffuse positivity with CD68 (Figure 9/C) and S100 (Figure 9/D) immunohistochemistry, while CD1a, langerin (CD207), and BRAF p.V600E reactions were negative. Focal strong positivity was detected with D5F3 ALK immunohistochemistry, but rearrangement affecting the *ALK* gene was not detected by FISH. The final histological diagnosis was

histiocytic neoplasm (non-Langerhans cell histiocytosis) with some morphological features of juvenile xanthogranuloma.

This research project was conducted in accordance with the Scientific and Research Committee of the Medical Research Council license IV/51-1/2022/EKU.

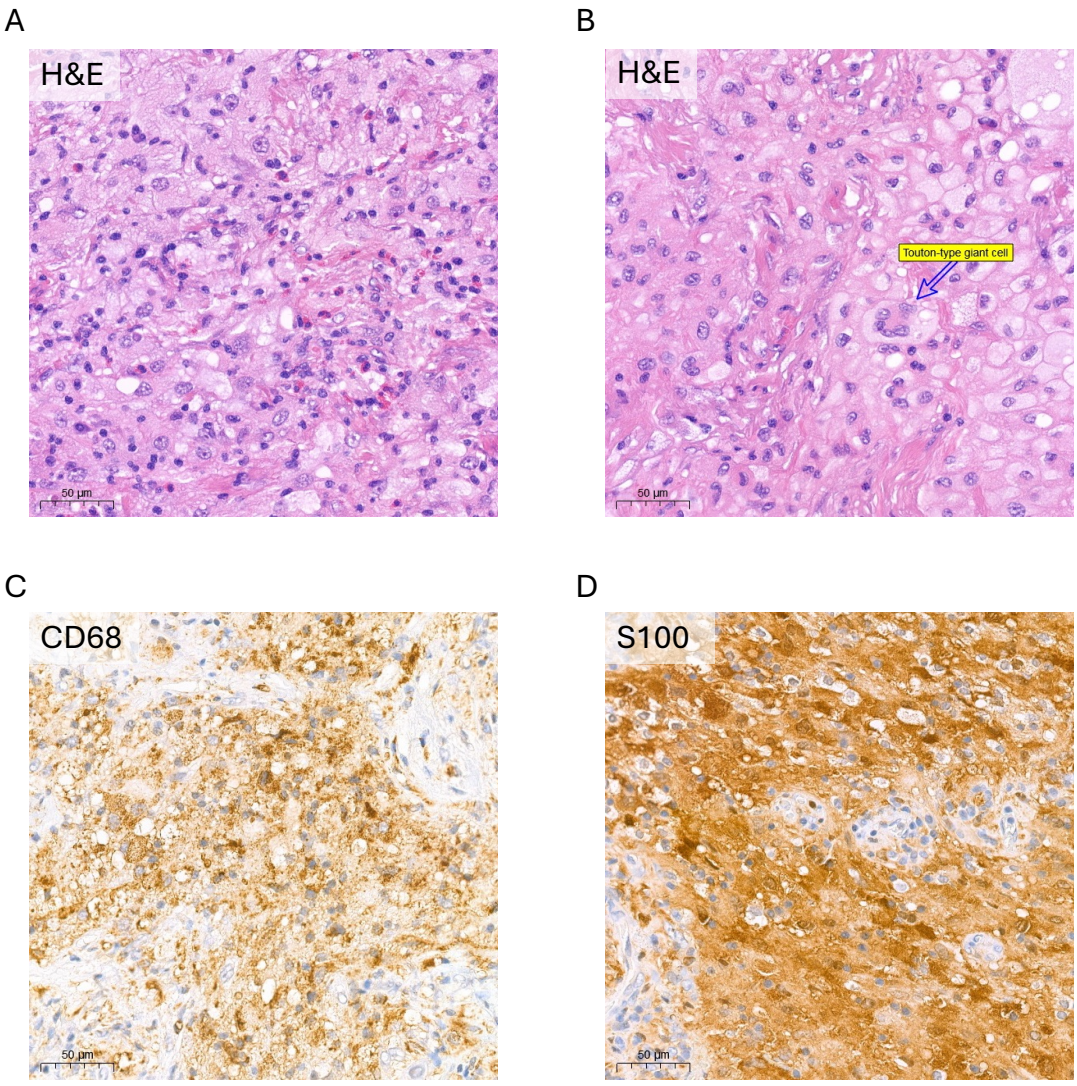

Figure 9. Histopathological and immunophenotypic characterization of the analyzed sample. Dense infiltrate of neoplastic histiocytes was detectable with H&E staining (A, B), along with Touton-type giant cells (B). Diffuse positive appearance was displayed using CD68 (C) and S100 (D) immunohistochemical reactions (300x magnification).

3.2.1. Nucleic acid extraction and quality assessment

Genomic DNA and total RNA were isolated from FFPE (formalin-fixed and paraffin-embedded) specimens using the QIAmp DNA FFPE Tissue Kit (QIAGEN GmbH, Hilden, Germany) and the High Pure FFPET RNA Isolation Kit (Roche Diagnostics GmbH, Mannheim, Germany). Estimation of tumor cell percentage of the sample was performed by histopathological examination prior to the isolation processes. DNA and RNA concentrations were measured using the Qubit dsDNA HS Assay and Qubit RNA HS Assay kits (Life Technologies Corporation, Eugene, Oregon, USA) on the Qubit 4 Fluorometer. 120 ng DNA in 52 µl volume was sheared (200 cycles, peak power: 75 Watt (W), duty factor: 10, treatment time: 510 sec, at 7°C setpoint) using a Covaris E220 Focused-ultrasonicator (Covaris, Woburn, Massachusetts, USA) and following the manufacturer's instructions. The size of double-stranded DNA fragments, and RNA molecules was confirmed after shearing using Tapestation 2200 (Agilent, Cheshire, UK).

3.2.2. Library preparation and next-generation sequencing

Library preparation workflow of Illumina TruSight Oncology 500 High Throughput assay was performed according to the manufacturer's protocol. Briefly, after end repair, A-tailing, adapter ligation, index PCR, as well as two hybridization and target-capture steps, libraries were amplified (16 PCR cycles), cleaned, quantified, normalized and pooled. Next-generation sequencing was performed on Illumina NextSeq 2000 platform, with 101-cycle, paired-end chemistry.

3.2.3. Bioinformatic analysis

Bioinformatic analysis was performed using the Illumina TruSight Oncology 500 Local App v2.1. Briefly, raw BCL files were downloaded, FASTQ generation was performed by bcl-convert software. The sequence-alignment to the hg19 reference genome was performed by the Burrows-Wheeler Aligner (BWA-MEM) along with SAMtools utility (64, 65). Read collapsing analysis was performed in order to accurately remove duplicate reads, marked by unique molecular identifiers (UMIs). Indel realignment and stitching were done by Gemini (66). Small variant calling was performed by Pisces, with the output being filtered by Pepe software component (67). Illumina Annotation Engine Nirvana

annotated the small variants using data from COSMIC (v84), ClinVar (2019-02-04), dbSNP (v151), 1000Genomes (Phase 3 v5a), gnomAD (2.1), RefSeq and Ensembl (VEP build 91) databases. Copy number variation calling was performed by CNV Robust Analysis For Tumors (CRAFT) software. For RNA-based analyses, each sample was downsampled to 30 million reads, then alignment was performed by Spliced Transcripts Alignment to a Reference (STAR) software to hg19 reference genome and GENCODE v19 reference transcriptome. Duplicates were marked by the Picard duplicate marking algorithm, and fusion calling was performed by Manta (68). Splice variants, tumor mutational burden and microsatellite instability (MSI) were determined by internally developed algorithms. For further clinical interpretation, QIAGEN Clinical Insight (QCI) Interpret software was used, which applies variant filtering and further annotations: pathogenicity scores, population-frequency, protein structure predictions, relevant clinical guidelines and therapeutic options for variants.

3.2.4. Immunohistochemistry

Immunohistochemistry (IHC) analyses of the tumor samples were performed on 3 μm thick sections from FFPE tissue blocks. The following primary antibodies were used: CD68 (Dako, Hamburg, Germany, 1:3000); S100 (Dako, 1:100); CD1a (Dako, 1:100); langerin (CD207) (Bio SB, Goleta, CA, USA, 1:50); BRAF p.V600E (Roche Diagnostics GmbH, Mannheim, Germany 1:100); ALK (Dako, 1:50); Cyclin D1 (Thermo Fisher Scientific, Waltham, MA, USA, 1:50); ROS1 (Roche Diagnostics GmbH, 1:2). Stainings were performed on Leica Bond-Max (Leica Biosystems, Danvers, MA) or Roche Ventana (Roche Diagnostics GmbH) automated immunostaining systems in accordance with the standard laboratory practice.

3.2.5. Sanger sequencing

Reverse transcription of RNA samples was performed using the High-Capacity cDNA Reverse Transcription Kit (Thermo Fisher Scientific), followed by bidirectional direct Sanger sequencing. Samples were sequenced on an ABI 3500 sequencing platform (Thermo Fisher Scientific) using custom-designed primers (forward primer: CACTCTCCCTAGCACCGAAG; reverse primer: ACACTTCTCCAAAGGCTCCA) in order to validate the *GIT2::ROS1* gene fusion.

4. RESULTS

4.1. Comprehensive DNA copy number aberration profiling in pediatric acute lymphoblastic leukemia

4.1.1. Frequency and distribution of chromosomal and subchromosomal copy number aberrations

In total, 1,398 CNAs including gross chromosomal alterations and subchromosomal lesions were detected in 244/260 (93.8%) diagnostic patient samples. On average, 5.4 CNAs were observed per patient with a mean of 2.5 subchromosomal aberrations. Ninety percent of whole chromosome changes were observed in patients bearing hyperdiploid karyotype with 4-14 affected chromosomes, predominantly extra copies of chromosomes 21, 6, X, 14, 18, 17, 4 and 10 (Figure 10). Gain of multiple copies was recurrently observed at chromosomes 21, X, 14 and 18. Modal chromosome number among the 82 patients harboring high-hyperdiploid karyotype ranged between 51 and 62 with a median of 55, while one patient displayed near-triploidy with 72 chromosomes.

Subchromosomal CNAs were identified in 208/260 (80.0%) patients with *VPREB1* deletion being the most common lesion occurring in 32.3% of the cases. Additional genes altered with a frequency of at least 5% in our patient cohort included various cell cycle control, lymphoid development, signaling or tumor suppressor genes such as *CDKN2A/B, ETV6, PAX5, IKZF1, MLLT3, TBL1XR1, BTG1, RB1, BTLA/CD200, CASP8AP2, RUNX1* as well as the PAR1 region (Table 4). Seventy percent of biallelic losses included the *VPREB1* and *CDKN2A/B* genes while over two-thirds of the multiple gains affected *RUNX1*. Approximately 8% of the subchromosomal CNAs were detected as subclonal aberrations which encompassed the *ETV6, PAX5, CDKN2A/B, IKZF1* and *VPREB1* genes in majority of the cases. Dosage quotient values indicating the fusion and amplification of the *NUP214* and *ABL1* genes were observed in two patients. Considering the genetic subtypes of pediatric B-ALL, the highest average numbers of subchromosomal aberrations (4.8-5.0 CNAs per patient) were observed in the *BCR::ABL1*-positive and iAMP21 subgroups, while the lowest values with 1.2-1.7 CNAs per patient were associated with hyperdiploidy and *TCF3::PBX1* fusion (Table 5).

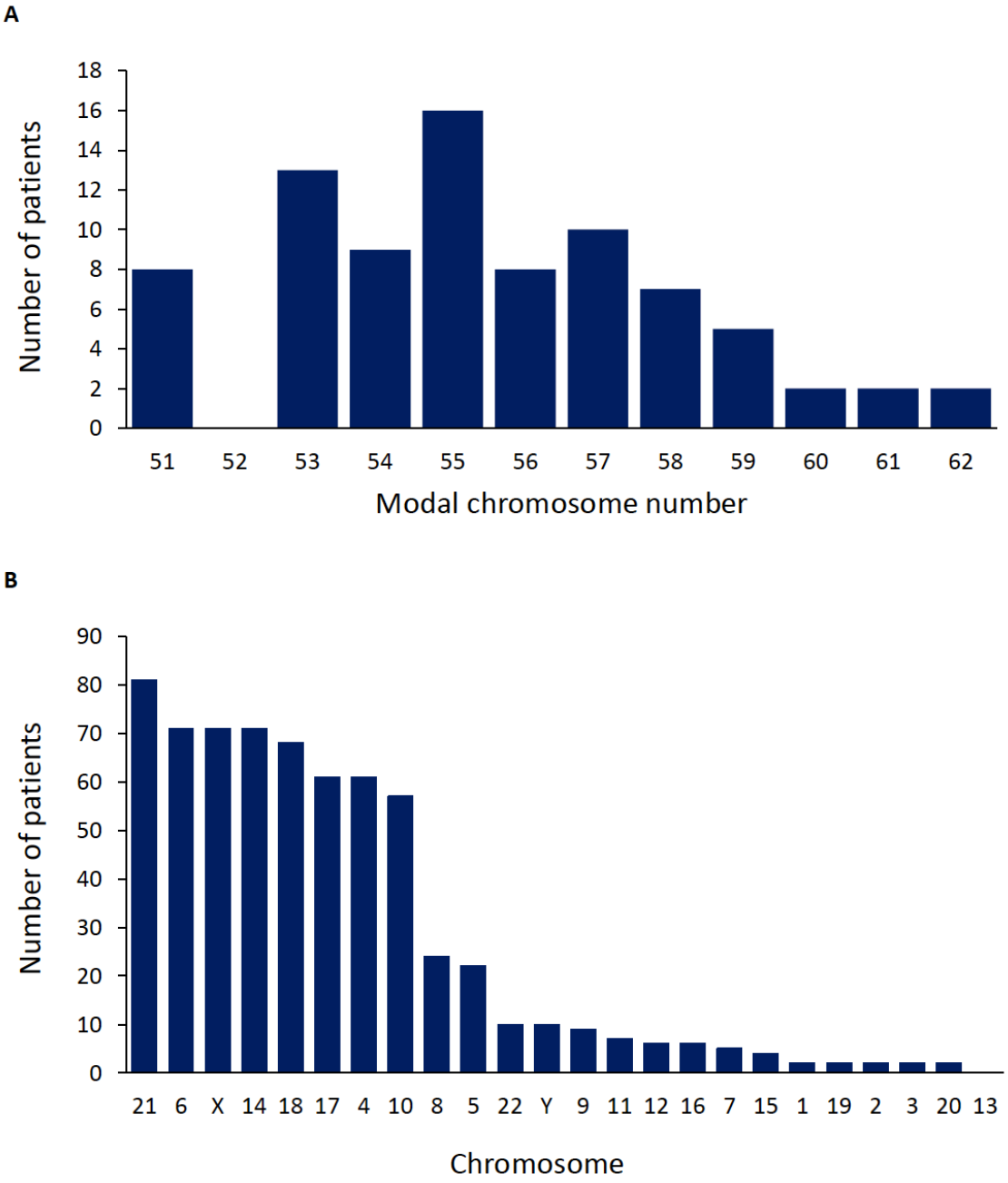

Figure 10. Modal chromosome number and frequency of whole chromosome gains in patients with high-hyperdiploid B-cell precursor acute lymphoblastic leukemia. Based on modal chromosome number determined by digitalMLPA (A), 82 patients displayed high-hyperdiploid karyotype with a chromosome number between 51 and 62. Multiple extra copies of chromosomes were counted as two-fold gains. The pattern of chromosomal gains (B) was dominated by extra copies of chromosomes X, 4, 6, 10, 14, 17, 18, and 21. In the diagnostic workflow, patients with hyperdiploid chromosome set were identified by karyotyping and/or DNA index measurement.

Table 4. Targets of subchromosomal copy number aberrations in diagnostic samples of 260 patients ranked in order of frequency.

Lesion	Gene	Total number of aberrations	Biallelic losses /multiple gains	Subclonal alterations
Loss	*VPREB1*	84	18	5
	CDKN2A/B	72	28	5
	ETV6	68	4	6
	PAX5	43	0	6
	IKZF1	34	1	5
	MLLT3	28	5	4
	PAR1	20	0	2
	TBL1XR1	19	1	0
	BTG1	17	0	0
	RB1	15	6	0
	BTLA/CD200	15	0	0
	CASP8AP2	15	0	2
	TP53	10	1	1
	CTCF	9	0	1
	NR3C1	8	0	2
	EBF1	5	0	0
	ERG	4	0	0
	LEF1	4	0	0
	PTEN	4	0	2
	NF1	3	0	0
	NR3C2	3	0	0
	EZH2	2	0	0
	SUZ12	2	0	0

	IKZF2	1	1	0
	NOTCH1	1	0	0
	PHF6	1	0	0
	PTPN2	1	0	0
Gain	*RUNX1*	23	11	1
	PHF6	11	4	0
	ABL1	6	1	0
	MYB	1	0	0

Table 5. Distribution of numerical and subchromosomal copy number aberrations across genetic disease subtypes.

Numerical chromosomal aberrations							
Genetic subtype	**Sum of CNAs**	**CNAs per patient**	**Copy number gains**	**Copy number losses**	**Multiple gains***	**Biallelic losses***	**Subclonal CNAs***
Hyperdiploidy	680	8.19	676	7	139	1	6
ETV6::RUNX1	33	0.48	22	11	2	0	2
BCR::ABL1	7	1.17	5	0	2	0	0
iAMP21	2	0.20	2	0	0	0	0
KMT2Ar	0	0.00	0	0	0	0	0
TCF3::PBX1	0	0.00	0	0	0	0	0
B-other	55	0.62	41	11	6	0	1
All samples**	761	2.93	734	27	147	1	8

Subchromosomal aberrations					
Genetic subtype	**Sum of CNAs**	**CNAs per patient**	**Copy number gains**	**Copy number losses**	**Subclonal CNAs***
Hyperdiploidy	96	1.16	38	57	14
ETV6::RUNX1	259	3.81	41	218	28
BCR::ABL1	29	4.83	4	25	4
iAMP21	50	5.00	21	29	1
KMT2Ar	13	3.25	0	13	1
TCF3::PBX1	5	1.67	2	3	0
B-other	199	2.24	29	170	17
All samples**	637	2.46	131	508	61

* Values represent a subset of copy number gains, copy number losses or sum of CNAs

** Values are not the sum of subtype-specific values due to three patients who showed features of two different subtypes

4.1.2. Co-segregation analysis of various CNAs and genetic subtypes in B-ALL

Simultaneous presence of various CNAs and B-ALL subgroup defining alterations was investigated in order to reveal potential associations between individual genetic lesions (Figure 11). The vast majority of mutual exclusivity or negative correlations was observed in the high-hyperdiploid subgroup, while the pairwise analyses revealed several significant positive correlations across various disease subtypes. The strongest positive associations were observed in the *ETV6::RUNX1* subgroup and included *ETV6* loss, *RUNX1* gain and *VPREB1* loss. Among patients with iAMP21, enrichment of *CDKN2A/B* loss and *RB1* deletion was observed. *IKZF1, MLLT3* and *CD200/BTLA* losses were associated with *BCR::ABL1* positivity, while *IKZF1* loss showed negative correlation with *ETV6::RUNX1* fusion and hyperdiploidy. Beyond that, *IKZF1* deletion showed significant co-occurrence with *TP53, BTG1* and *MLLT3* as well as with deletion of the *PAR1* region.

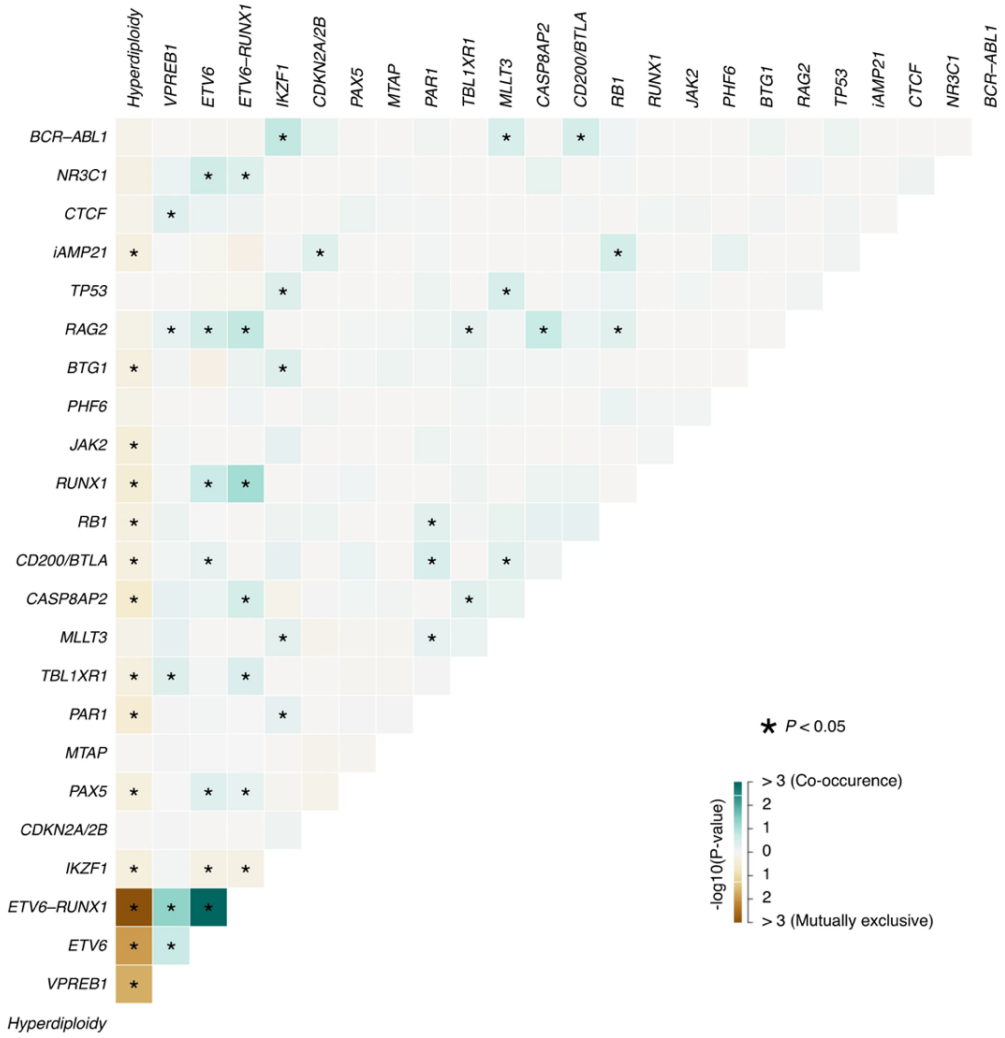

Figure 11. Co-segregation analysis of genetic subgroup defining alterations and copy number aberrations affecting genes recurrently altered in pediatric B-ALL. Co-occurrence and mutual exclusivity between various B-ALL subgroup defining alterations and/or detected copy number aberrations are labeled with green and brown colors, respectively. Significant ($p < 0.05$) associations revealed by pair-wise Fisher's exact test are marked with asterisks.

4.1.3. Hyperdiploidy and prognosis

Whole chromosome gains were investigated individually and in combinations to identify specific patterns associated with favorable outcome among patients with high-hyperdiploid karyotype as revealed or confirmed by digitalMLPA. Simultaneous survival rate analyses using the Kaplan-Meier method unraveled multiple single, double and triple trisomies as markers of good risk, mainly including various combinations of

chromosomes 4, 6, 10, 17 and 18, and excluding gains of chromosomes 5 and 20. Due to multiple statistical comparisons of these combinations, results were corrected using the Bonferroni method, after which double trisomy of chromosomes 4 and 6 remained as the only marker significantly associated with superior outcome within the high-hyperdiploid subgroup (Figure 12).

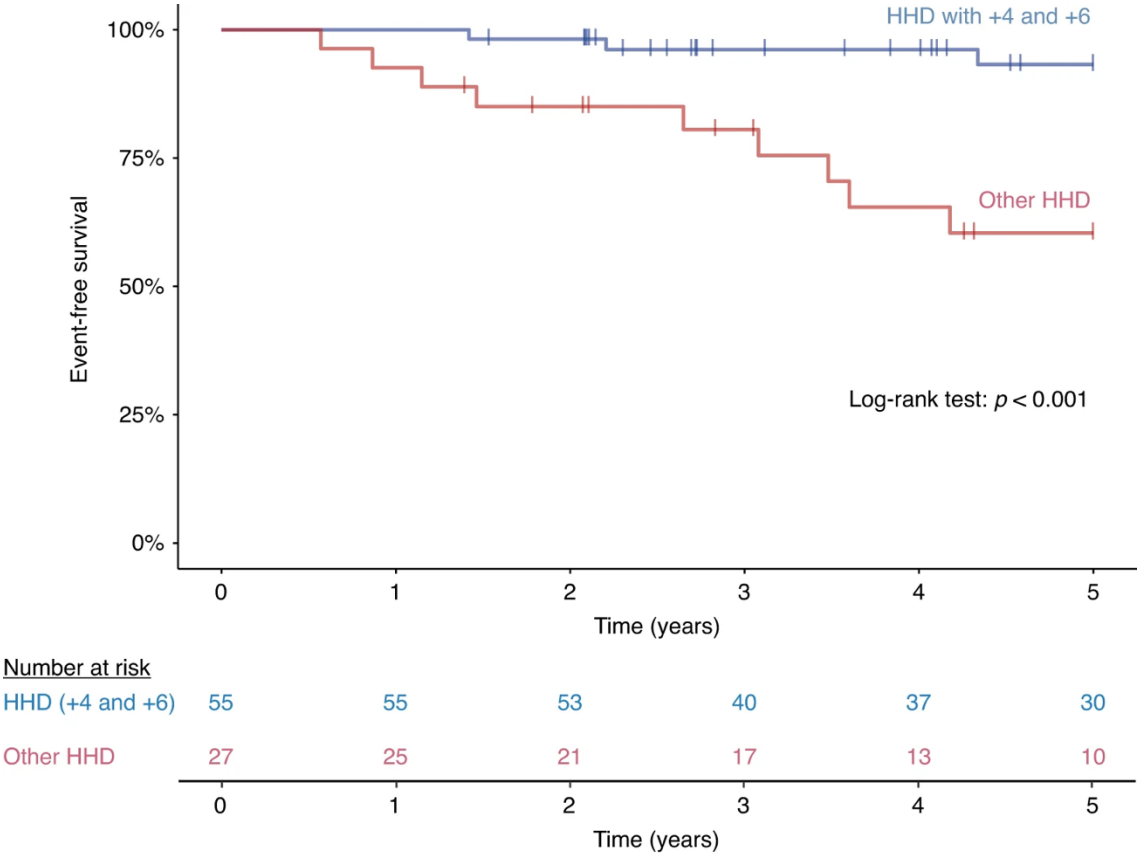

Figure 12. Event-free survival of high-hyperdiploid patients with presence or absence of double trisomy affecting chromosomes 4 and 6. High-hyperdiploid (HHD) patients with extra chromosomes of 4 and 6 showed higher estimated 5-year EFS rate than other high-hyperdiploid patients in our cohort (93.2% vs. 60.4%).

4.1.4. IKZF1 status and its prognostic value

The D007 digitalMLPA probemix covers all exons of the *IKZF1* gene with two probes, as well as regions located approximately 4 and 2 kilobases upstream of the coding sequences, enabling a fine mapping of deletions affecting the *IKZF1* gene. In patients harboring *IKZF1* loss, 10 different patterns of deletion were observed, predominantly exons 4-7 and exons 1-7 losses, as well as deletion of the entire gene including the upstream region (Figure 13). Notably, we observed a non-random distribution of *IKZF1*^{del}

and *IKZF1*^{plus} statuses across patients displaying different patterns of *IKZF1* deletion. Eight out of nine patients with exons 4-7 loss and 6/7 patients with upstream region/exons 1-8 (i.e. whole *IKZF1*) deletion showed *IKZF1*^{plus} CNA profile. On the other hand, all patients with exon 1-7 deletion belonged to the *IKZF1*^{del} group, without meeting the criteria of *IKZF1*^{plus}.

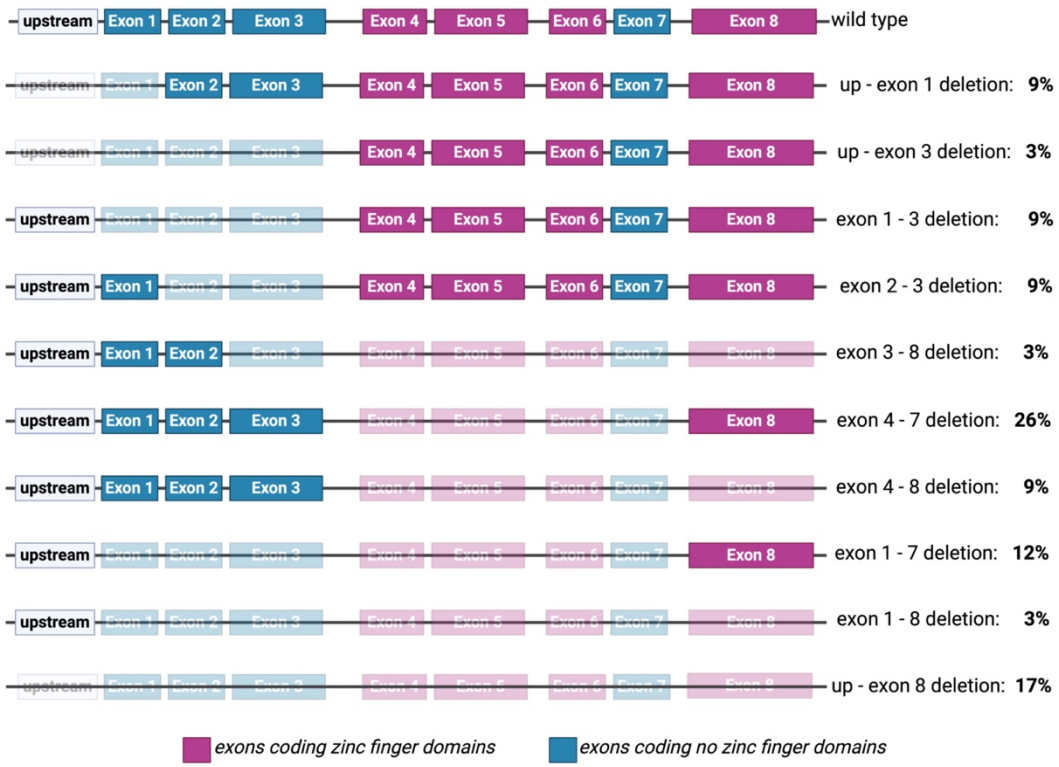

Figure 13. Patterns and frequencies of *IKZF1* gene deletions in children with B-ALL. Ten different deletion patterns were observed in 34 patients, affected exons/regions are indicated with blurred boxes. Exon 4-7 loss and upstream region/exon 1-8 deletion showed strong association with *IKZF1*^{plus} CNA profile, while exon 1-7 deletion was almost exclusively detected among patients harboring *IKZF1* loss but without meeting the criteria of *IKZF1*^{plus}.

By analyzing the prognostic value of *IKZF1* status in our patient cohort, a decreasing rate of EFS was observed in patents with normal vs *IKZF1*^{del} vs *IKZF1*^{plus} genotype; however, the difference between the latter two categories did not reach statistical significance (Figure 14).

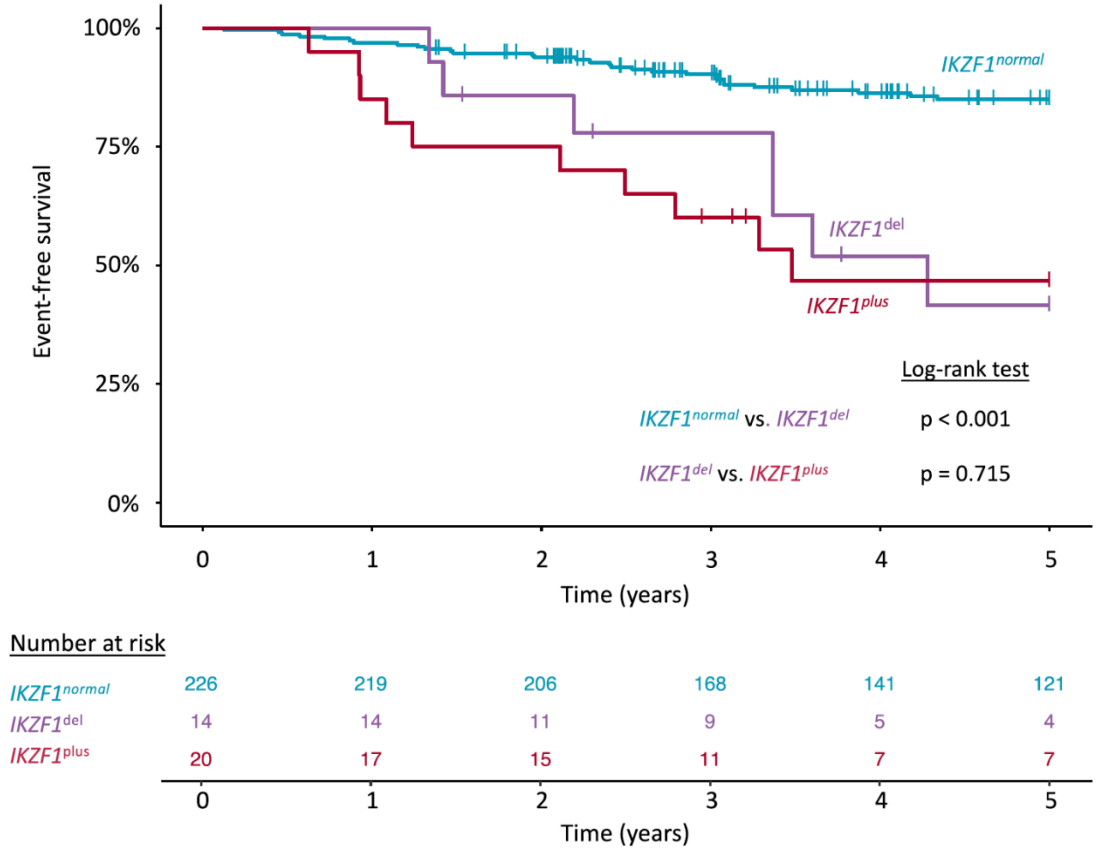

Figure 14. Event-free survival of patients with *IKZF1*^{normal}, *IKZF1*^{del} and *IKZF1*^{plus} genotypes. Patients displaying *IKZF1* deletion with or without meeting the criteria of *IKZF1*^{plus} showed shorter 5-year event-free survival as compared with patients with intact *IKZF1* alleles (*IKZF1*^{normal}: 85.0%, *IKZF1*^{del}: 41.6%, and *IKZF1*^{plus}: 46.7%). As in the original study by *Stanulla et al 2018*, (44) presence of *IKZF1* deletion as well as at least one additional deletion in the *PAX5, CDKN2A/B* or PAR1 genes/regions in the absence of *ERG* deletion was considered as *IKZF1*^{plus} genotype.

We hypothesized that co-evaluation of *IKZF1* status and additional cytogenetic features interdependently may improve the *IKZF1*-driven prognostic risk assessment. In order to generate these novel subgroups, we combined the *IKZF1* status with cytogenetic categories defined and applied successfully in previous studies (Figure 15) (32, 45, 46), which eventually allowed for distinguishing three prognostic groups (IKAROS-low, IKAROS-medium and IKAROS-high) with significantly different 5-year EFS (Figure 16).

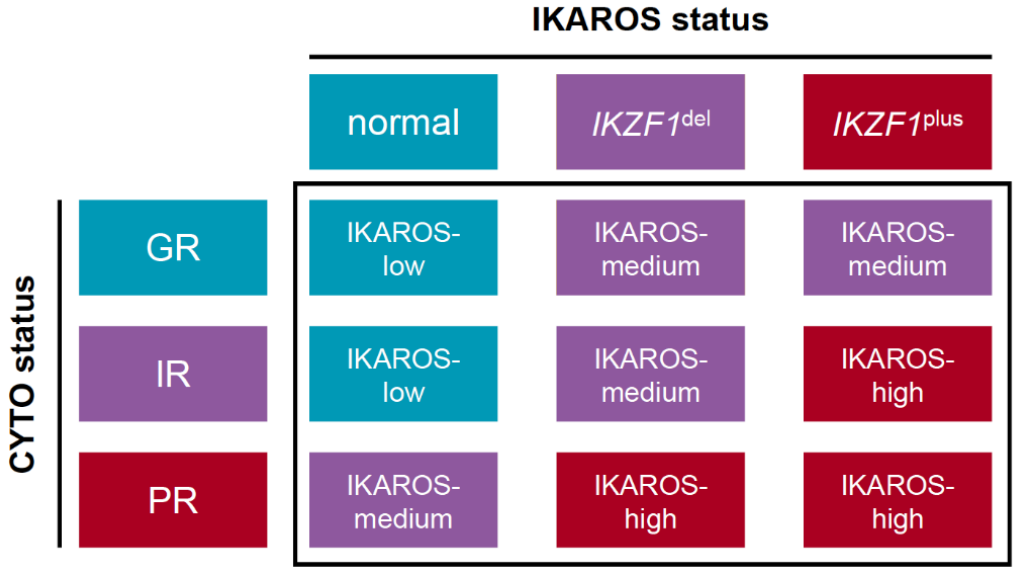

Figure 15. Combined risk groups based on cytogenetic (CYTO) features and *IKZF1* status. Cytogenetic risk groups were determined according to the UKALL system by *Hamadeh et al 2019* (46). GR: good risk; IR: intermediate risk; PR: poor risk. *IKZF1* status is referred as *IKZF1*^{plus} if in addition to *IKZF1* loss, the patient harbored *PAX5, CDKN2A/B* or PAR1 deletion, without concurrent *ERG* loss.

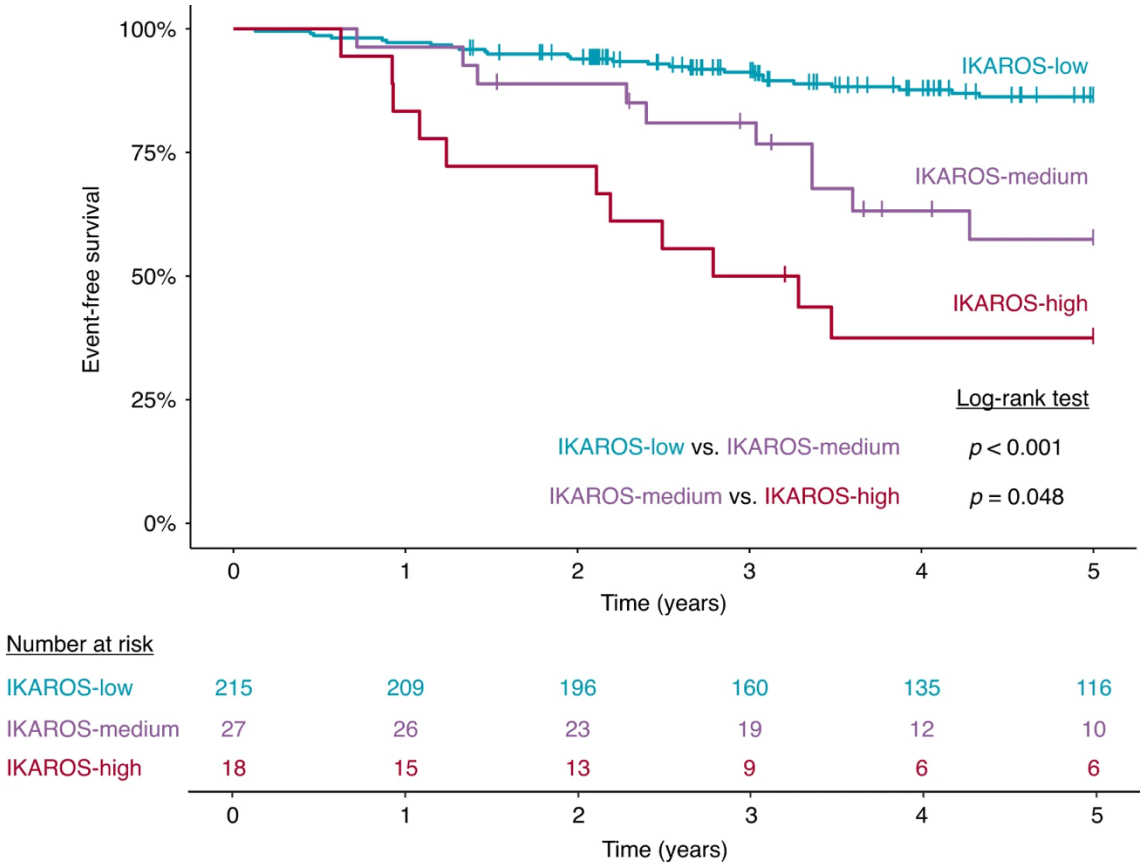

↑ **Figure 16: Event-free survival of 260 patients classified by combined cytogenetic and *IKZF1* copy number status.** Risk groups were determined as outlined in Figure 15. Patients in the IKAROS-low, IKAROS-medium and IKAROS-high groups showed an estimated 5-year EFS rate of 86.3%, 57.4% and 37.5%, respectively.

4.1.5. Integrative genetic classification for personalized risk assessment

In order to establish a highly personalized risk assessment of patients with B-cell precursor ALL, we introduced a novel classification called *PersonALL*, which flexibly takes account of the unique composition of aberrations in individual patients. First, prognostic significance of all disease-relevant, recurrent genetic aberrations detected by digitalMLPA or by conventional approaches such as karyotyping and FISH was evaluated in our patient cohort using univariate Cox proportional hazard models. Second, aberrations with a frequency of >1.5% and a Cox model hazard ratio of >1.5 or ≤0.66 were selected and used for calculating patient-specific cumulative scores. The scoring system proportionally weighted individual cytogenetic aberrations and subchromosomal CNAs as outlined in Table 6.

Table 6. Prognostic influence of genetic aberrations assessed by univariate Cox regression models.

Genetic aberration*	Hazard ratio	Score
IKZF1 loss	4.82E+00	-4
BCR::ABL1 fusion	4.60E+00	-4
PTEN loss	4.49E+00	-4
P2RY8::CRLF2 fusion	4.30E+00	-4
KMT2A rearrangement	4.20E+00	-4
LEF1 loss	4.10E+00	-4
iAMP21	2.50E+00	-2
HHD** without +4 and +6	2.30E+00	-2

TP53 loss	2.00E+00	-2
MLLT3 loss	1.90E+00	-1
B-other	1.80E+00	-1
CDKN2A/B loss	1.51E+00	-1
ERG gain	1.43E+00	0
PAX5 loss	1.40E+00	0
PAR1 loss	1.40E+00	0
RUNX1 gain	1.20E+00	0
PDGFRB loss	1.17E+00	0
JAK2 loss	1.10E+00	0
MTAP loss	1.10E+00	0
BTG1 loss	1.10E+00	0
CD200/BTLA loss	1.10E+00	0
EBF1 loss	9.40E-01	0
terminal 5q loss	9.20E-01	0
NR3C1 loss	6.90E-01	0
VPREB1 loss	6.90E-01	0
RB1 loss	6.00E-01	+1
CTCF loss	5.90E-01	+1
ETV6 loss	3.00E-01	+2
HHD** with +4 and +6	2.40E-01	+4
ETV6-RUNX1 fusion	2.40E-01	+4
TBL1XR1 loss	2.40E-01	+4

ERG loss	1.13E-07	+4
RAG2 loss	3.90E-08	+4
PHF6 gain	3.82E-08	+4
CASP8AP2 loss	3.70E-08	+4

* Aberrations with <1.5% abundance were excluded. Scores were assigned based on hazard ratio ranges: 0.00-0.25: +4, 0.26-0.33: +3, 0.34-0.50: +2, 0.51-0.66: +1, 1.51-2.00: -1, 2.01-3.00: -2, 3.01-4.00: -3, >4.01: -4. ** HHD: High hyperdiploidy.

Patient-specific cumulative scores generated from the prognostic value of single genetic lesions distinguished four prognostic subgroups with excellent (score: ≥4), good (score: 0-3), high (score: -1 to -4) and ultra-poor risk (score: ≤ -4), demonstrating significantly different 5-year EFS rates (Figure 17).

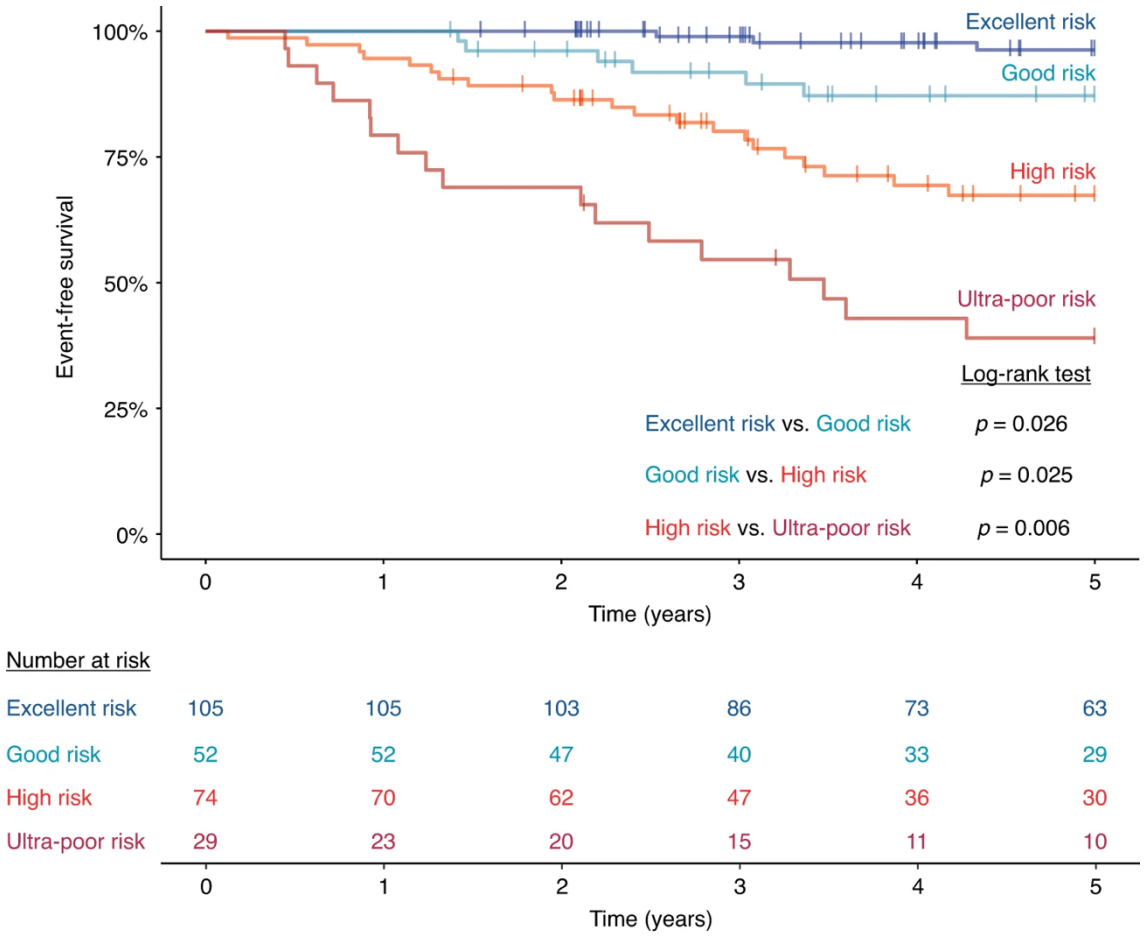

↑ **Figure 17: Event-free survival of 260 patients with B-cell precursor ALL, classified according to patient-specific composition of all disease-relevant aberrations associated with prognostic significance in our patient cohort.** Excellent, good, high and ultra-poor risk groups showed an estimated 5-year EFS rate of 96.3%, 87.2%, 67.4% and 39.0%, respectively. Patient-specific scores were calculated as outlined in Table 6.

The excellent, good, high and ultra-poor risk groups comprised 40.4%, 20.0%, 28.5% and 11.1% of the patients, respectively. The excellent risk group almost exclusively contained patients with *ETV6::RUNX1* fusion or high-hyperdiploid karyotype with common double trisomy of chromosomes 4 and 6. An increased fraction of B-other cases coupled with reduced representativity of *ETV6::RUNX1* positivity and high-hyperdiploidy was observed in the good-risk group. In the high-risk group, almost two-thirds of the patients were classified as B-other, while the ultra-poor risk group was enriched for *BCR::ABL1* gene fusion, and other gene fusions including *CRLF2* and *ABL* class aberrations characteristic of Ph-like signature and iAMP21 genotype (Figure 18).

Performance of *PersonALL* was validated on an independent cohort of 606 patients included in the TARGET ALL phase 1 pilot and phase 2 expansion studies, using a scoring scheme identical to the one applied at our in-house discovery cohort. Comparison of the excellent, good, high and ultra-poor risk groups consisting of 30.0%, 24.1%, 39.6% and 6.3% of the patients, respectively, demonstrated significantly different 5-year EFS rates (Figure 19/A). In addition, we tested this novel risk assessment method on the merged dataset comprising relevant information from all patients (n = 866) included in the validation cohort and in our discovery cohort. The difference in 5-year EFS across the risk groups showed even higher statistical significance than observed in the validation cohort, thus providing further confirmation on the value and robustness of our newly introduced prognostic classifier (Figure 19/B).

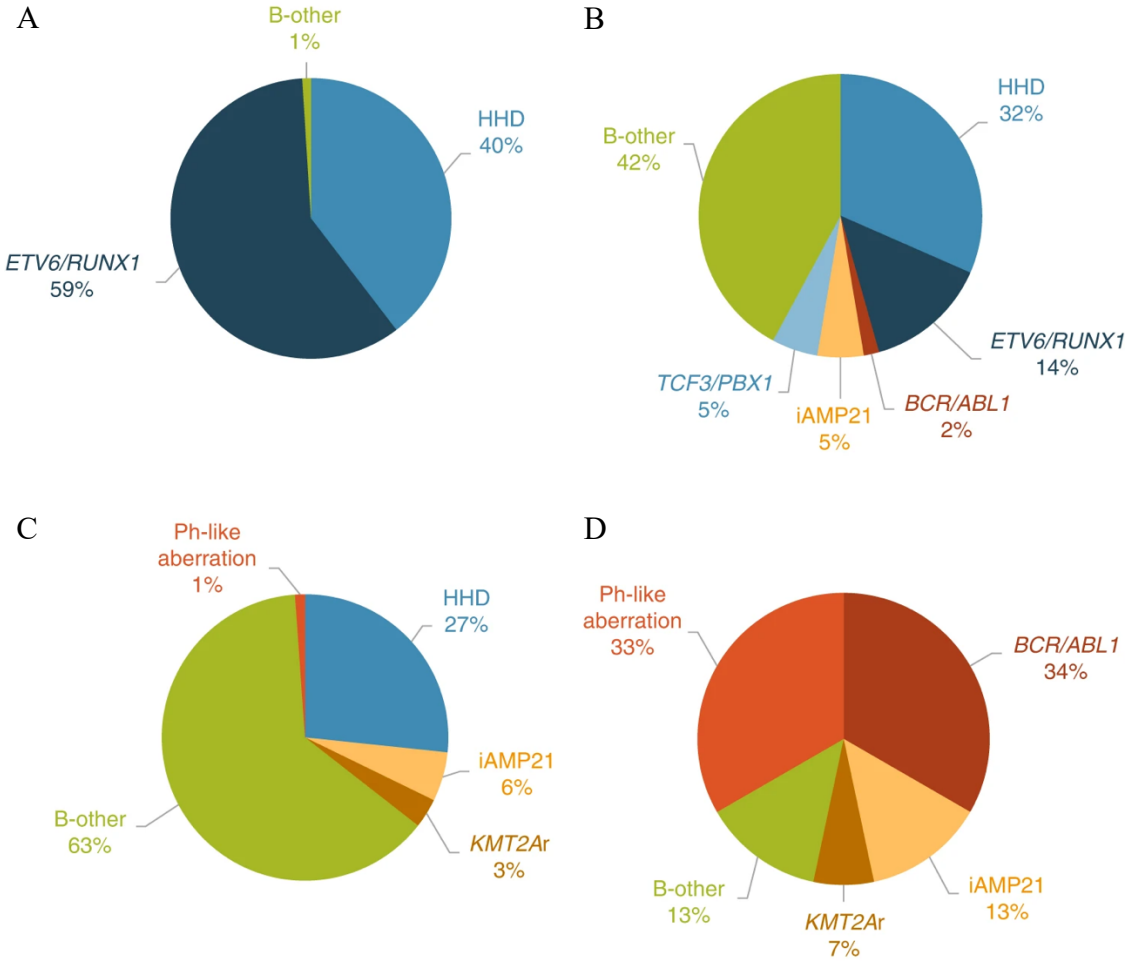

Figure 18: Distribution of cytogenetic subtypes across four risk groups determined based on non-overlapping ranges of patient specific cumulative scores generated from the prognostic value of single genetic lesions. The excellent risk group (A) almost exclusively comprised patients with *ETV6::RUNX1* gene fusion or high-hyperdiploid (HHD) karyotype. The good (B) and the high-risk (C) groups were dominated by patients who classified as B-other in the current study. Two-thirds of the patients in the ultra-poor risk group (D) carried *BCR::ABL1* fusion or alterations characteristic of the Ph-like subtype, with an additional one-fifth of the children in this group harboring *KMT2A* rearrangement or iAMP21 genotype.

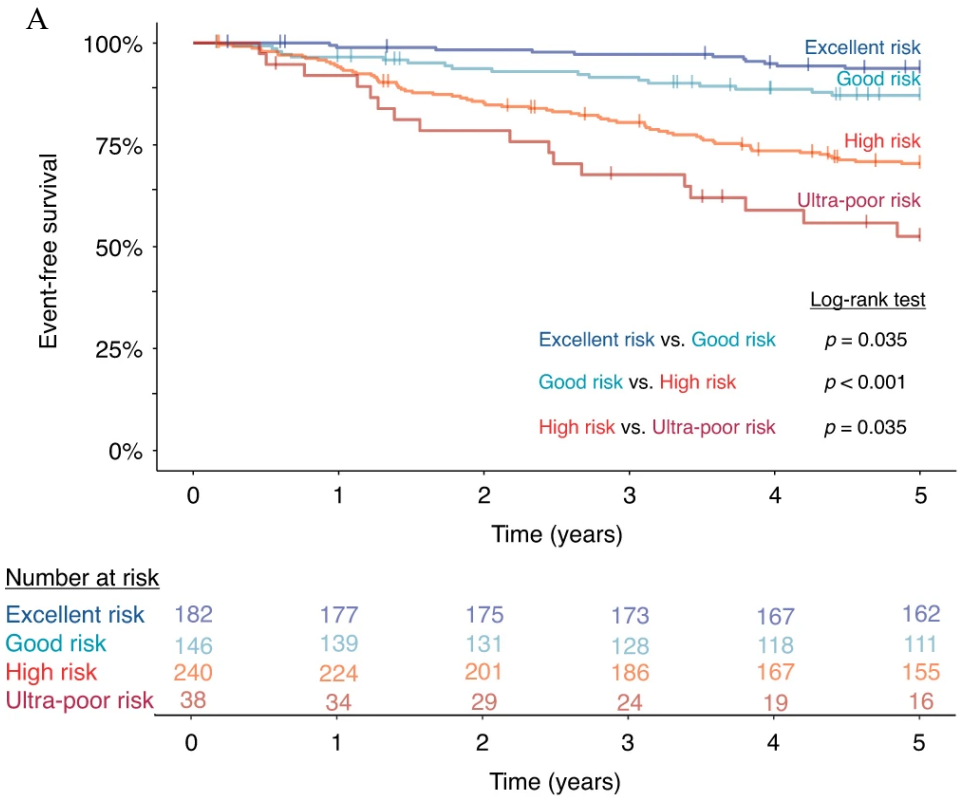
A
100%
75%
50%
25%
0%
Event-free survival
Excellent risk
Good risk
High risk
Ultra-poor risk
Log-rank test
Excellent risk vs. Good risk p = 0.035
Good risk vs. High risk p < 0.001
High risk vs. Ultra-poor risk p = 0.035
0
1
2
3
4
5
Time (years)
Number at risk
Excellent risk 182 177 175 173 167 162
Good risk 146 139 131 128 118 111
High risk 240 224 201 186 167 155
Ultra-poor risk 38 34 29 24 19 16
0
1
2
3
4
5
Time (years)

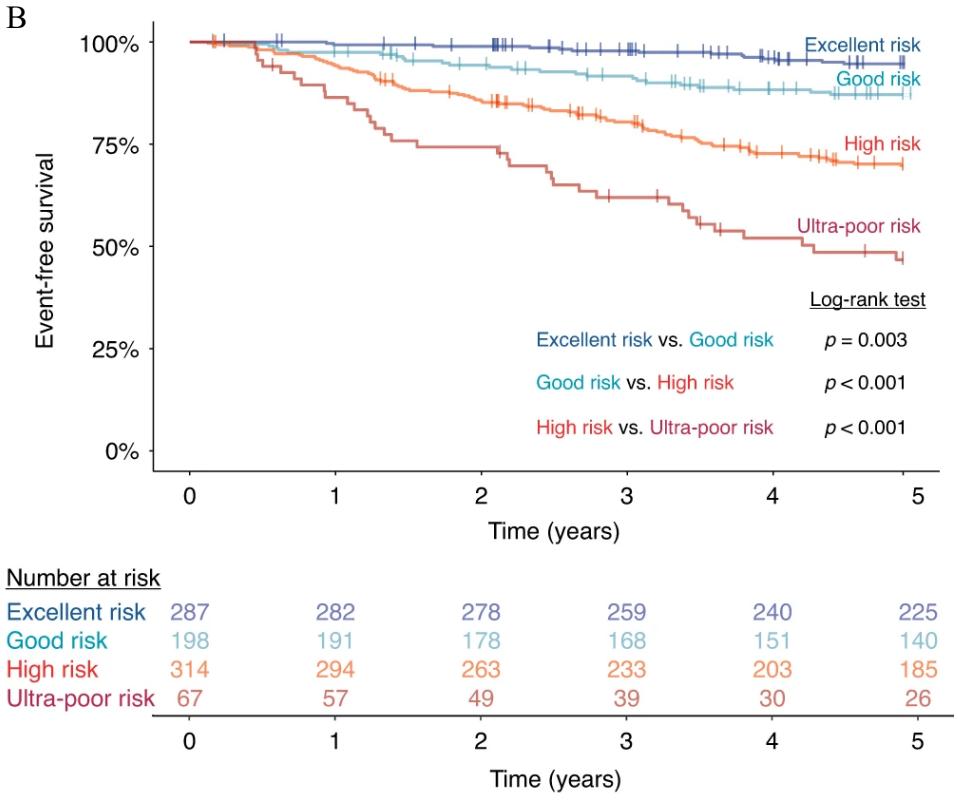
B
100%
75%
50%
25%
0%
Event-free survival
Excellent risk
Good risk
High risk
Ultra-poor risk
Log-rank test
Excellent risk vs. Good risk p = 0.003
Good risk vs. High risk p < 0.001
High risk vs. Ultra-poor risk p < 0.001
0
1
2
3
4
5
Time (years)
Number at risk
Excellent risk 287 282 278 259 240 225
Good risk 198 191 178 168 151 140
High risk 314 294 263 233 203 185
Ultra-poor risk 67 57 49 39 30 26
0
1
2
3
4
5
Time (years)

↑**Figure 19. Validation of *PersonALL*, a novel classification approach assigning patients to four prognostic subgroups based on highly individualized cumulative scores reflecting the weighted impact of all detected and prognostically relevant genetic aberrations**. (A) Event-free survival of 606 patients with B-cell precursor ALL included in the TARGET ALL phase 1 pilot or phase 2 expansion studies. Excellent, good, high and ultra-poor risk groups showed an estimated 5-year EFS rate of 93.8%, 87.2%, 70.4% and 52.5%, respectively. (B) Event-free survival of 866 (260 + 606) patients with B-cell precursor ALL included in the merged discovery (in-house) and validation cohort. Excellent, good, high and ultra-poor risk groups showed an estimated 5-year EFS rate of 94.7%, 87.2%, 69.8% and 46.8%, respectively.

4.2 Discovery, comprehensive genomic profiling and effective molecularly targeted therapy of the novel type of histiocytic neoplasm driven by *GIT2::ROS1* gene fusion

4.2.1. Identification of the first histiocytic neoplasm with ROS1 gene fusion by comprehensive genomic profiling

Histopathological diagnosis of the investigated case was histiocytic neoplasm (non-Langerhans cell histiocytosis) with some morphological features of juvenile xanthogranuloma, however histology and immunophenotype of the tumor overlaps with Erdheim-Chester disease, and ALK-positive histiocytosis. NGS-based comprehensive genomic profiling was performed on the FFPE specimen using the Illumina TruSight Oncology 500 assay. Bioinformatic analyses identified a novel *GIT2::ROS1* fusion involving the *GIT2* (12q24.11; exon 16) and *ROS1* (6q22.1; exon 36) loci (Figure 20/A). The detected fusion was validated using *ROS1* break-apart FISH probe (Figure 20/B) and Sanger sequencing of the fusion transcripts (Figure 20/C). Comprehensive genomic profile of the analyzed FFPE sample revealed several small nucleotide variants (SNVs), small insertions, deletions (InDels) as well as low-level copy number gains, all of which are considered as variants with unknown clinical significance (Table 7). Therefore, the detected *GIT2::ROS1* fusion was the only pathogenic variant, hence driver genetic event in the sample (Table 7). In order to validate the gene expression of the detected fusion and the highest-level CNA (low level copy number gain of *CCND1*) on protein level, we performed ancillary immunohistochemical studies, which showed diffuse, weak to moderate cytoplasmic positivity with the D4D6 ROS1 antibody (Figure 21/A),

and a widespread strong nuclear labeling with Cyclin D1, encoded by the *CCND1* gene (Figure 21/B).

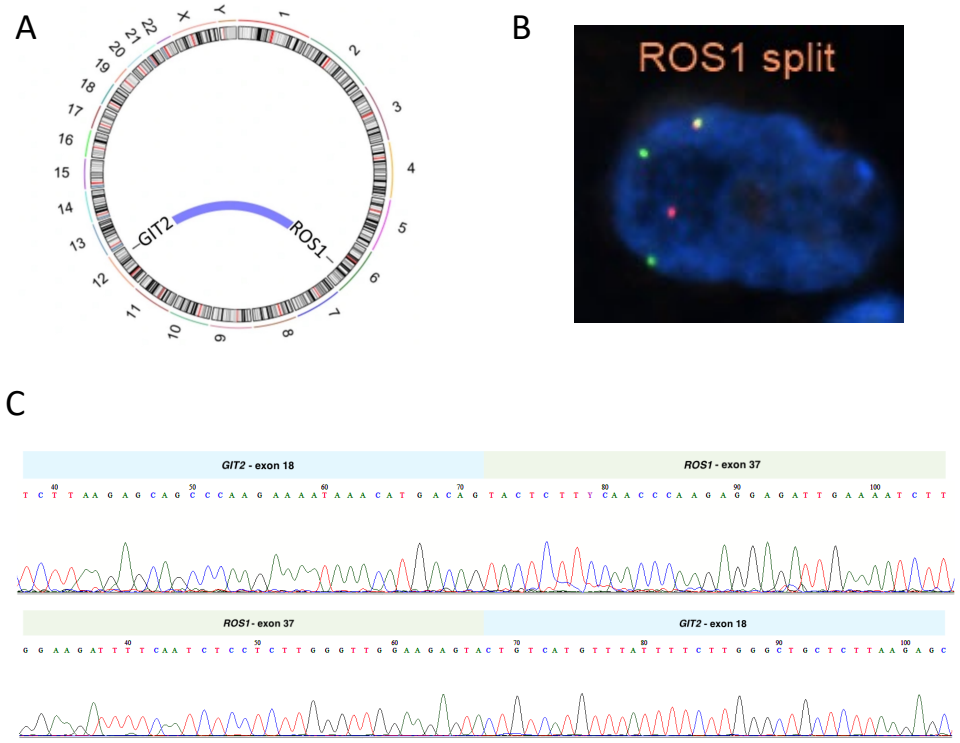

Figure 20. Detection of the novel *GIT2::ROS1* gene fusion by independent molecular methods. (A) Circos plot displays the genomic translocation between the 12q24.11 (*GIT2*) and 6q22.1 (*ROS1*) loci resulting in the aforementioned gene fusion. (B) FISH reaction applying *ROS1* break-apart probes visualizes the translocation of *ROS1* gene. (C) Electropherograms obtained by bidirectional Sanger sequencings display successful validation of the *GIT2::ROS1* fusion.

4.2.2. Effective therapeutic targeting of the driver ROS1 gene fusion and favorable clinical outcome

Postoperative MRI showed no or mild changes in the size of known lesions, but novel sacral (S1-2) neuroforaminal foci appeared. Bone scintigraphy and trephine biopsy were negative.

↓Table 7. Main elements of the comprehensive genomic profile of the first *ROS1* translocated histiocytic neoplasm case. Beyond the pathogenic *GIT2::ROS1* gene fusion the listed genetic variants and factors were detected with unknown clinical significance.

Gene	Chr	SNVs, InDels					Classification
		Genomic ref. seq.	cDNA ref. seq.	AA ref. seq.	VAF	Transcript ID	
CSF1R	5	g.149459890C>T	c.317G>A	p.R106Q	46.0% of 1332 reads	NM_005211.4	Uncertain Significance
CTNNA1	5	g.138145882C>A	c.457C>A	p.Q153K	44.0% of 596 reads	NM_001903.5	Uncertain Significance
DIS3	13	g.73347874C>T	c.1187G>A	p.R396Q	44.0% of 863 reads	NM_014953.5	Uncertain Significance
FOXP1	3	g.71247357_7124735 9delTGC	c.174_176delGCA	p.Q60del	2.44% of 1271 reads	NM_032682.6	Uncertain Significance
GATA2	3	g.128204960G>C	c.481C>G	p.P161A	44.0% of 1090 reads	NM_032638.5	Uncertain Significance
H3C8	6	g.26271208T>C	c.405A>G	p.R135R	57.0% of 706 reads	NM_003534.3	Uncertain Significance
NF2	22	g.30070923C>T	c.1439C>T	p.T480M	46.0% of 443 reads	NM_000268.4	Uncertain Significance
POLD1	19	g.50919872G>A	c.2959G>A	p.D987N	49.0% of 384 reads	NM_002691.4	Uncertain Significance
SPEN	1	g.16255086G>A	c.2351G>A	p.R784H	46.0% of 641 reads	NM_015001.3	Uncertain Significance
TET1	10	g.70405539_70405 541delATAinsGTG	c.3053_3055delATAi nsGTG	p.N1018_K1019delins SE	43.0% of 634 reads	NM_030625.3	Uncertain Significance
TFRC	3	g.195779048T>A	c.2048A>T	p.Y683F	3.31% of 272 reads	NM_001128148.3	Uncertain Significance
Fusion							
ROS1::GIT2		Read depth: 262					Likely pathogenic
CNVs							
KIT	4	Low-level copy number gain (copy number: 3.1)					Pathogenic
RET	10	Low-level copy number gain (copy number: 3.9)					Pathogenic
CCND1	11	Low-level copy number gain (copy number: 4.1)					Pathogenic
FGF3	11	Low-level copy number gain (copy number: 3.1)					Pathogenic
MYCN	2	Low-level copy number gain (copy number: 3.4)					Pathogenic
PDGFRB	5	Low-level copy number gain (copy number: 3.3)					Pathogenic
FGF4	11	Low-level copy number gain (copy number: 3.2)					Uncertain Significance
Tumor Mutational Burden: TMB-low (1.6 Mutations/Megabase)							
Microsatellite Status: MSI-low							

SNVs: small nucleotide variants, InDels: insertions-deletions, CNAs: copy number aberrations, TMB: tumor mutational burden, MSI: microsatellite instability

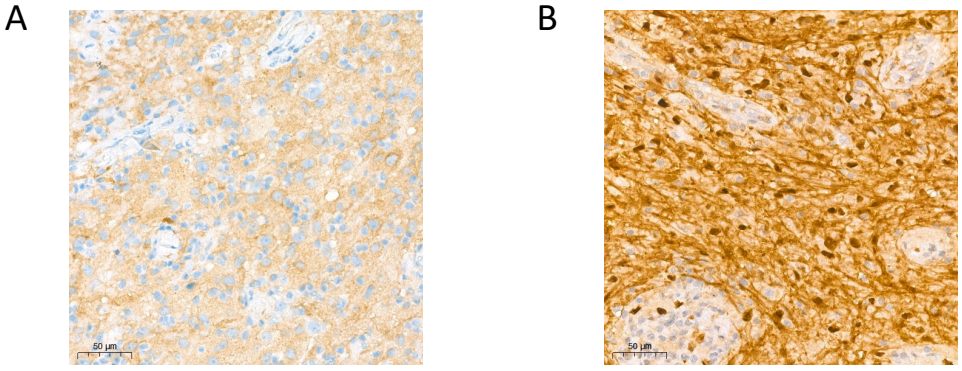

Figure 21. Immunohistochemical analysis of the gene expression of *ROS1* and *CCND1* genes. Immunohistochemical reaction of D4D6 ROS1 antibody (A) showed diffuse, weak to moderate cytoplasmic positivity; widespread strong nuclear labeling with Cyclin D1 (B), encoded by the *CCND1* gene (300x magnification).

The treatment was started with the DAL-HX 90 chemotherapeutic regimen including alternating "A" (etoposide, ifosfamide and methotrexate) and "B" (vinblastine, etoposide and methotrexate) blocks, completed with intrathecal triple therapy (methotrexate, prednisolone and cytarabine) and subcutaneous cladribine (Figure 22). Following these, entrectinib treatment was applied as a maintenance therapy based on the molecular report, with an off-label indication. Control MRI performed during the chemotherapy as well as 1 month and 4 months following the introduction of entrectinib showed radiologically stable disease. In the second month of entrectinib treatment, clear improvement of visual disturbances was clinically detectable, although a visual field defect of the right eye was suspected and the nystagmus was still present. Six months following the entrectinib treatment initiation, by the time of the submission of the publication (Bedics, Csóka et. al.: Novel actionable *ROS1::GIT2* fusion in non-Langerhans cell histiocytosis with central nervous system involvement, Acta Neuropathologica, 2022), the visual field defect was no longer evident, and the patient could show parts of tiny objects and imitate the examiner's gesticulation (69).

↓Figure 22. Timeline demonstrating the diagnostic procedures and therapeutic interventions during the clinical course of the reported case in months from the initial presentation (CNS: central nervous system, ETP: etoposide, IFO: ifosfamide, i.th.: intrathecal, i.v.: intravenous, MRI: magnetic resonance imaging, MTX: methotrexate, pred.: prednisolone, VBL: vinblastine)

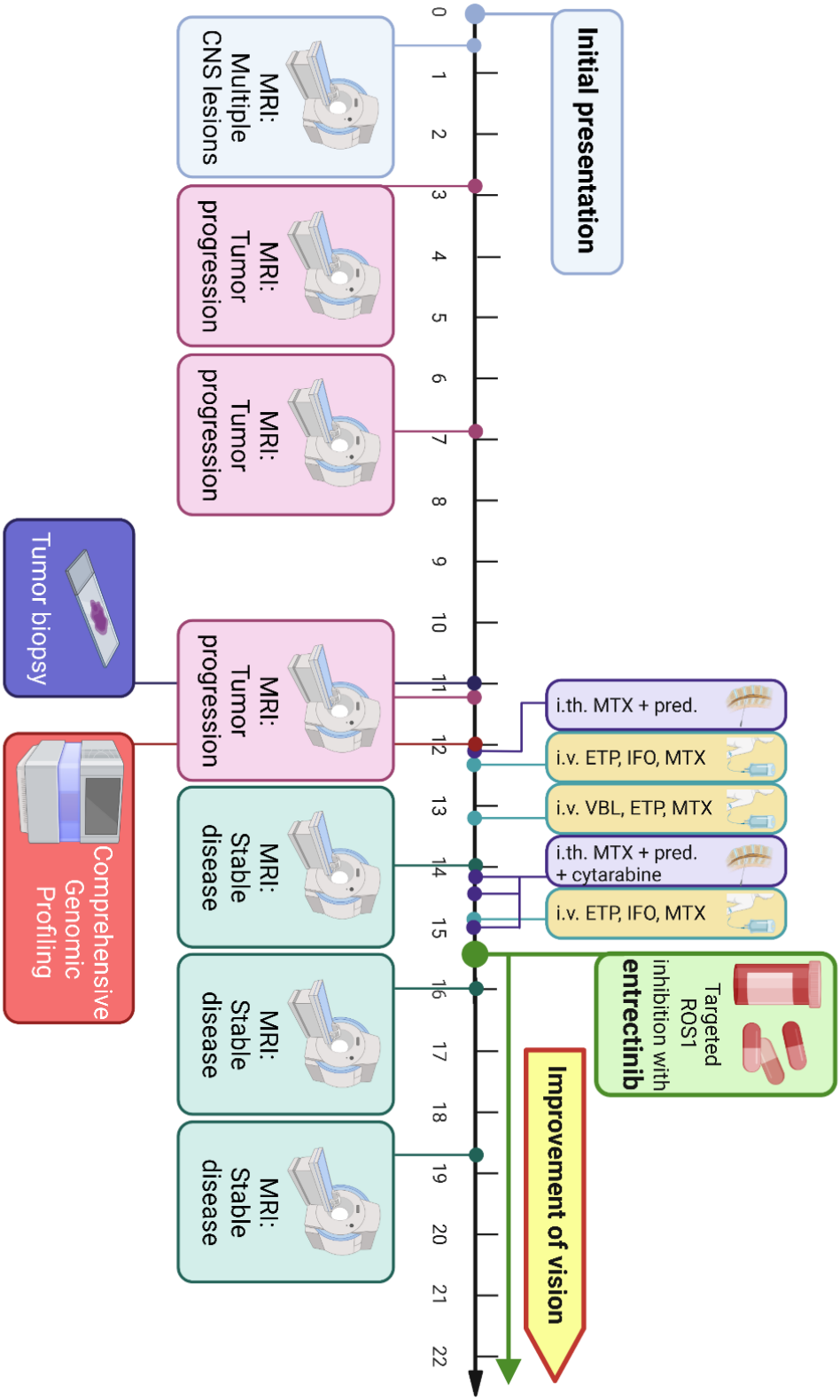
Initial presentation
MRI: Multiple CNS lesions
MRI: Tumor progression
MRI: Tumor progression
Tumor biopsy
MRI: Tumor progression
Comprehensive Genomic Profiling
MRI: Stable disease
MRI: Stable disease
MRI: Stable disease
i.th. MTX + pred.
i.v. ETP, IFO, MTX
i.v. VBL, ETP, MTX
i.th. MTX + pred. + cytarabine
i.v. ETP, IFO, MTX
Targeted ROS1 inhibition with entrectinib
Improvement of vision
0
1
2
3
4
5
6
7
8
9
10
11
12
13
14
15
16
17
18
19
20
21
22

5. DISCUSSION

Studies applying molecular genetic profiling methods focusing on malignant hematopoietic and lymphoid diseases have provided highly valuable data, which contributed to the development of novel classification systems, leading to more personalized and effective treatment strategies for patients diagnosed with these neoplasms (7, 14, 47, 57). My doctoral research focused on certain malignant hematopoietic and lymphoid diseases of childhood, applying recent next-generation sequencing-based molecular techniques and related bioinformatic methods. During this research, we performed comprehensive DNA copy number aberration profiling utilizing the novel digitalMLPA method on a large cohort of Hungarian children diagnosed with B-cell precursor ALL, which allowed us to detect certain combinations of CNAs that have clear prognostic value, and to develop a conceptually novel genetic scoring guide for B-cell precursor ALL. In addition, utilizing comprehensive genomic profiling, we discovered a novel driver genetic constellation of histiocytic neoplasms.

5.1. Comprehensive profiling of disease-relevant DNA copy number aberrations determined by digitalMLPA in pediatric acute lymphoblastic leukemia

In this research project, we applied digitalMLPA, a robust high-throughput method for screening disease-relevant CNAs in a nation-wide cohort of Hungarian children diagnosed with B-ALL. While the general feasibility of our approach had previously been demonstrated (32), the significantly larger patient population in the current analysis allowed us to go far beyond a simple validation of observations made before. Detection of chromosomal and large subchromosomal CNAs along with exon-level mapping of focal driver aberrations provided prognostically relevant results by (*i*) unveiling chromosomal gains associated with the most favorable EFS in the high-hyperdiploid subgroup, (*ii*) identifying *IKZF1* deletion patterns specifically associated with *IKZF1*^{del} and *IKZF1*^{plus} genotypes, (*iii*) facilitating the establishment of a cytogenetically aware patient classification based on IKAROS status, and most importantly, (*iv*) allowing us to design and successfully test a conceptually novel prognostic classifier called *PersonALL* which dynamically takes into account all possible

combinations of potentially co-segregating genetic aberrations screened by digitalMLPA and/or more conventional methods.

Molecular and cytogenetic characterization of the diagnostic samples provided evidence of representativity of our patient cohort in terms of genetic subgroups, frequency of chromosomal and subchromosomal driver aberrations, as well as co-segregation of key recurrent alterations. For example, we observed enrichment of *IKZF1* deletions in the *BCR-ABL1* positive subgroup, common *ETV6* and *TBL1XR1* losses in patients harboring *ETV6-RUNX1* fusion, co-occurrence of *IKZF1* losses with deletions in the PAR1 and 9p regions or in the *BTG1* gene, and frequent emergence of *RB1* deletion among patients with iAMP21 genotype (44, 70-75). The extended number of patients and the digital karyotyping probe subset of the D007 digitalMLPA probemix allowed us to identify specific chromosomal gains associated with superior outcome among patients with high-hyperdiploid karyotype, efficiently supporting the robust implementation of our personalized genetic classifier.

5.2. Copy number aberrations of *IKZF1* defined by digitalMLPA may refine IKAROS-related prognostics

Deletion of the *IKZF1* gene encoding the transcription factor IKAROS is observed in 15-20% of children with B-ALL and it is reported to be associated with inferior clinical outcome with a range of different treatment protocols (42, 76-79). *Stanulla* et al. also defined *IKZF1*^{plus}, a very poor, measurable residual disease (MRD)-dependent prognostic subgroup consisting of patients who in addition to *IKZF1* loss, harbor *PAX5*, *CDKN2A/B* or PAR1 deletion, without concurrent *ERG* loss (44). Distribution of *IKZF1* deletion patterns in our study (Figure 13) resembles previously published data (76), with exon 4-7 deletion (isoform 6 - loss of DNA binding region) being the most common subtype, followed by deletions affecting all exons with or without the analyzed upstream region (80). Various types of *IKZF1* loss confer inferior EFS regardless of their frequency and extension albeit at quite different levels of significance when compared with matching wild-type controls (81). Although the number of patients with *IKZF1* loss was limited in our study, we observed a strong association of specific deletion patterns with either *IKZF1*^{del} or *IKZF1*^{plus} genotype. Importantly, almost all

patients harboring exon 4-7 deletion showed *IKZF1*^{plus} genotype which can provide a plausible explanation why this lesion is typically associated with very adverse clinical outcome, even if patients with *IKZF1* loss are exclusively analyzed (81). This observation certainly needs validation in larger patient cohorts prospectively or retrospectively.

In terms of prognosis, our patients displaying *IKZF1* loss with or without fulfilling the criteria of *IKZF1*^{plus} showed significantly shorter EFS compared to patients without *IKZF1* deletion (Figure 14), nevertheless the difference between the two *IKZF1* altered subgroups were not significant, similar to a recent observation by Felice et al. (82). Therefore, we integrated *IKZF1* status (*IKZF1*^{normal}, *IKZF1*^{del} and *IKZF1*^{plus}) as revealed by digitalMLPA with cytogenetic classes, thus creating a cytogenetics aware interpretation of *IKZF1* allelic status (Figure 15), which substantially improved the risk assessment for our patients by distinguishing three prognostic groups with significantly different 5-year EFS (Figure 16).

5.3 Development of *PersonALL*, a conceptually novel prognostic classifier and its potential contribution to clinical decision-making

Risk assessment based on molecular features of leukemic blasts is gaining increased importance in the clinical stratification of children with B-ALL. Several recurrent CNAs including whole chromosome aberrations and focal alterations have prognostic and/or predictive significance which has led to the incorporation of CNAs into various risk classifiers (32, 41, 44-46). While co-segregation of different driver aberrations was reported in large-scale genomic studies, flexible prognostic classification approaches adaptively considering the specific combination of genetic lesions in individual patients have not been established to date.

Pediatric ALL develops via multi-step acquisition of molecular and cytogenetic aberrations, and a subset of alterations shows enriched co-segregation or mutual exclusivity as it has also been demonstrated in our study (Figure 11). Nevertheless, the specific compositions of detectable driver aberrations vary substantially between individual patients which is only considered to a limited extent even by the most recent prognostic classifiers (32, 41, 44, 46). Therefore, we explored the feasibility of an

alternative risk assessment approach which adaptively, at individual patient level takes into account all aberrations screened and found to be prognostically relevant in our patient cohort. This integrative method that has also been validated on a large independent patient cohort (N = 606), provides important guidance not only in cases where favorable and adverse prognostic markers are simultaneously present, represented by 25% of our patients, but also allows for a more weighted prognostic classification of each individual patient and hence a refined risk assessment in general. Of note, the conventional classification applied in the ALL IC-BFM protocols failed to define three risk groups with significantly different 5-year EFS rates in our patient cohort, while four distinct subgroups could be determined using *PersonALL*, clearly demonstrating the added value of our conceptually novel classifier (Figure 17). The relationships between risk groups defined by the ALL IC-BFM protocols and by the *PersonALL* method are outlined in Figure 23. Excellent, good and high-risk groups of the *PersonALL* classification included patients from all three ALL IC-BFM risk groups and the ultra-poor risk group also involved patients originally classified in different ALL IC-BFM groups, evidently reflecting the more comprehensive principles applied in our new classifier.

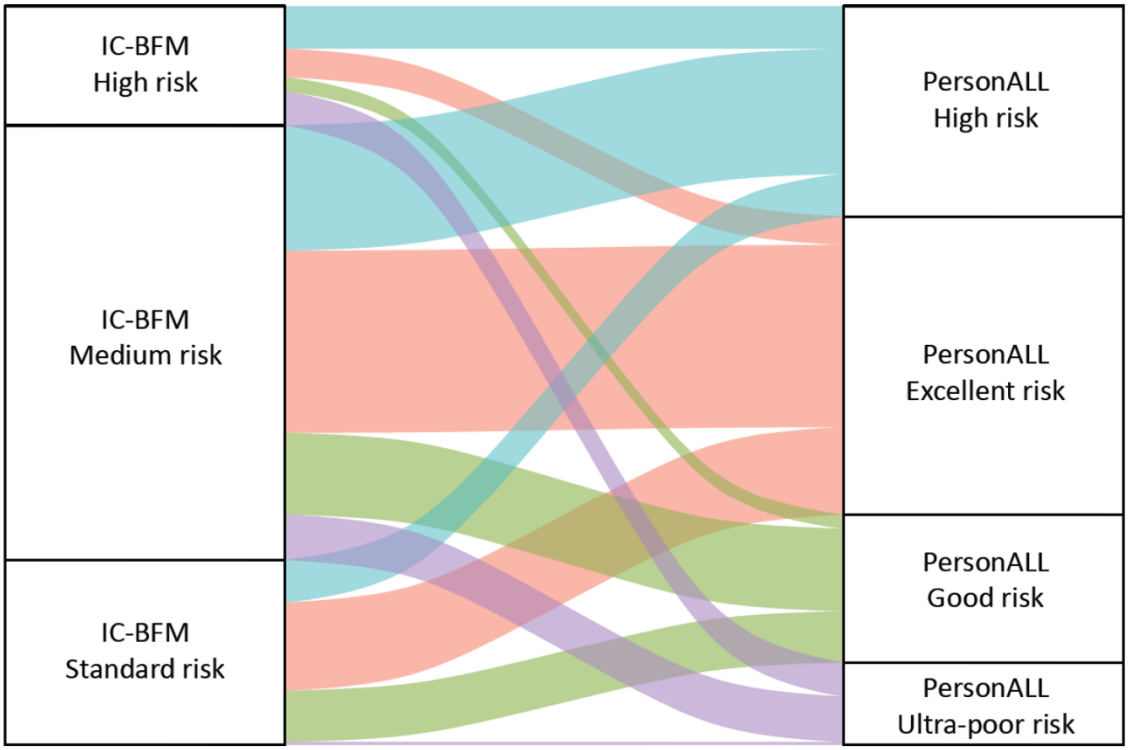

↑**Figure 23. Assignment of patients stratified based on IC-BFM protocols to novel prognostic subgroups of *PersonALL* defined by non-overlapping ranges of personalized cumulative scores reflecting the weighted impact of all detected and prognostically relevant genetic aberrations.** *PersonALL* considers all combinations of co-segregating genetic alterations, providing a more comprehensive and more refined patient stratification.

Distinguishing four subgroups based on personal composition of genomic lesions as described above may have a direct impact on the clinical management of children with B-ALL in the future. Sixty percent of patients were classified into two prognostically favorable risk groups with a 5-year EFS above 85%, while the other 40% of patients were divided over two risk groups with inferior outcomes (5-year EFS below 70%).

Considering the EFS rates of approximately 80-90% in pediatric ALL in the developed countries (83), we may draw some strategic conclusions with regard to the anti-leukemia treatment in these four prognostic subgroups. Reduced therapeutical intensity or longer intervals between consecutive treatment blocks may be considered for patients with 'excellent' prognosis to avoid short- and long-term toxicities. MRD monitoring and MRD-driven therapy optimization should be a main focus at patients classified in the 'good' and, particularly, in the 'high-risk' groups. A high-resolution MRD follow-up with patient-specific molecular marker screening and monitoring would be warranted in the 'high-risk' group, especially in those countries where the main MRD assessment method is flow cytometry. In cases with 'ultra-poor' risk profile, treatment intensification or change in therapeutic approach (e.g. immunotherapy, cell therapy or molecularly targeted therapy) could potentially be initiated even if the early MRD response is promising, due to a very high risk of relapse during and after the first-line ALL treatment.

The current study has some limitations partially coming from the unavailability of MRD data at a significant number of patients which prevented the evaluation of an MRD-guided classifier in this retrospective analysis. Of note, our integrative genetic scoring guide aiding the classification of patients into distinct prognostic groups could still successfully be established even without accounting for the MRD status. Another shortcoming is the low abundance of some typically uncommon but prognostically relevant alterations (e.g. *TCF3::PBX1* and *NUP214::ABL1* fusions) which hampered the incorporation of

those into the newly developed classifier. Nevertheless, we do believe our research provides a novel and innovative risk assessment method for patients with pediatric B-ALL, and the proposed approach, also validated on a second patient cohort, can be further refined using prospectively collected large patient populations which on one hand will overcome the limitations mentioned above, on the other hand will allow for additional independent validation of our patient-specific prognostic classifier.

5.4 Discovery and effective treatment of the first histiocytic neoplasm with *ROS1* gene fusion

The group of histiocytic neoplasms affecting the central nervous system includes rare entities with diverse clinicopathological features and variable prognosis. Diagnostics of these entities is frequently complicated, since not only histological, but molecular characteristics may be overlapping (48). Molecularly targeted therapies have been shown to be highly efficacious in this disease group with genetic variants affecting the MAPK pathway being the most common events (84). Of note, the recently described, predominantly pediatric ALK-positive histiocytosis shows durable sensitivity for ALK inhibitors as well (49, 50, 52).

We reported a pediatric case of histiocytic neoplasm affecting the CNS and harboring a novel *ROS1* fusion (*GIT2::ROS1*) identified by comprehensive genomic profiling (Figure 20, Table 7). The novel genetic finding was validated with independent molecular methods such as FISH and Sanger-sequencing, moreover, ROS1 immunohistochemical reaction showed overexpression at the protein level (Figure 20, Figure 21).

Histology and immunophenotype of the tumor overlap with Erdheim-Chester disease, juvenile xanthogranuloma and ALK-positive histiocytosis. Cyclin D1 overexpression has been reported in both Rosai-Dorfman-Destombes disease (85) as well as ALK-positive histiocytosis and is related to both MAPK/ERK and PI3K/AKT/mTOR pathway activation (52). Considering the similarity of ALK and ROS1 signal transduction, positivity of cyclin D1 in our *ROS1*-rearranged case is not surprising and underlies the utility of this marker in the diagnostics of histiocytic neoplasms.

ROS1 is a receptor tyrosine kinase with poorly characterized physiological functions. However, fusions affecting this gene have been described in several benign and malignant tumors including a subset of non-small-cell lung carcinomas (NSCLC) (86). These rearrangements are characterized by diverse partner genes and breakpoints found between exon 32 and 36 of *ROS1* resulting in constitutive activity of the kinase domain (87). *GIT2* encodes an ADP ribosylation factor (ARF) GTPase activating protein (GAP). *GIT2::BRAF* and *GIT2::PDGFRB* fusions were described in pilocytic astrocytoma (88) and chronic myeloproliferative disorders (89), respectively, with breakpoints in exon 12 of *GIT2*. Altered protein-protein interactions related to ankyrin and ARF-GAP domains of *GIT2* are the presumed mechanisms of oncogene activation (89). The *GIT2::ROS1* gene fusion identified in our patient has not been reported previously, but the breakpoints suggest a mechanism similar to the ones mentioned above.

Entrectinib is a small molecular tyrosine kinase inhibitor with efficient blood-brain barrier penetration and favorable side-effect profile. The compound was approved by the Food and Drug Administration of the United States (FDA) and the European Medicines Agency (EMA) for the treatment of adult patients with NSCLC harboring *ROS1* fusion (90). The radiological stabilization and significant clinical improvement in our case suggest the utility of this compound in *ROS1*-rearranged histiocytosis as well.

To the best of our knowledge, we reported the first case of successful disease control using entrectinib treatment of a histiocytic neoplasm with novel *GIT2::ROS1* fusion. Although this association needs to be confirmed in additional cases, our observation raises the possibility to expand the classification of histiocytic neoplasm with the novel *ROS1* driver alteration, and this study clearly highlights the utility of CGP in histiocytic neoplasms.

6. CONCLUSIONS

Novel findings of my thesis are the following:

1. We determined a comprehensive disease-relevant DNA copy number aberration profile applying digitalMLPA in a large cohort of Hungarian children diagnosed with B-ALL (N=260, representing patient number equivalent with 4-year-incidence in Hungary) for the first time.
2. We observed a strong association of specific deletion patterns with either *IKZF1*^{del} or *IKZF1*^{plus} genotype. Importantly, almost all patients harboring exon 4-7 deletion showed *IKZF1*^{plus} genotype leading to the loss of DNA binding region of the protein, which can provide a plausible explanation why this lesion is typically associated with very adverse clinical outcome. Moreover, all patients with exon 1-7 deletion belonged to the *IKZF1*^{del} group, without meeting the criteria of *IKZF1*^{plus}.
3. We integrated *IKZF1* status (*IKZF1*^{normal}, *IKZF1*^{del} and *IKZF1*^{plus}) as revealed by digitalMLPA with cytogenetic classes for the first time, thus creating a cytogenetics aware interpretation of *IKZF1* allelic status, which substantially improved the risk assessment for our patients by distinguishing three prognostic groups with significantly different 5-year EFS.
4. We introduced a conceptually novel genetic risk classification approach called *PersonALL*, which assigns patients to prognostic subgroups based on highly individualized cumulative scores reflecting the weighted impact of all relevant aberrations detected in a particular patient. This newly developed prognostic classifier which flexibly considers all possible combinations of screened and potentially co-segregating genetic alterations provides a more refined, hence more personalized risk assessment for children with B-ALL.
5. We discovered the first histiocytic neoplasm driven by a novel *ROS1* gene fusion (*GIT2::ROS1*) identified by comprehensive genomic profiling and validated by various orthogonal molecular laboratory methods.
6. We provided the first evidence of efficacious ROS1-inhibitor treatment in the patient diagnosed with *ROS1*-translocated histiocytic neoplasm, with significant improvement of clinical symptoms and achievement of a radiologically stable disease.

7. SUMMARY

My doctoral research focused on molecular genetic profiling using next-generation sequencing-based methods and bioinformatic approaches of certain pediatric malignant hematopoietic and lymphoid diseases, such as pediatric acute lymphoblastic leukemia and histiocytic neoplasms.

We performed a comprehensive screening for disease-relevant CNAs in a cohort of Hungarian patients diagnosed with pediatric B-ALL using digitalMLPA. The generated CNA profiles were combined with cytogenetic data for risk assessment. We integrated *IKZF1* status (*IKZF1*^{normal}, *IKZF1*^{del} and *IKZF1*^{plus}) with cytogenetic classes, thus creating a cytogenetics aware interpretation of *IKZF1* imbalance for the first time, which substantially improved the risk assessment for our patients by distinguishing three prognostic groups with significantly different 5-year EFS. We also introduced a conceptually novel patient classification approach called *PersonALL*, which assigns patients to prognostic subgroups based on highly individualized cumulative scores reflecting the weighted impact of all relevant aberrations detected in a particular patient. This newly developed prognostic classifier, which flexibly considers all possible combinations of screened and potentially co-segregating genetic alterations, provides a more refined, hence more personalized risk assessment for children with B-ALL.

We discovered the first histiocytic neoplasm driven by a novel *ROS1* gene fusion (*GIT2::ROS1*) identified by comprehensive genomic profiling and validated by a range of different molecular laboratory methods. Moreover, we reported the first evidence of efficacious ROS1-inhibitor (entrectinib) treatment in the patient diagnosed with *ROS1*-translocated histiocytic neoplasm, with significant improvement of clinical symptoms and achievement of a radiologically stable disease. Although this association needs to be confirmed in additional cases, our finding raises the possibility to expand the classification of histiocytic neoplasms with the novel *ROS1* driver alteration. Our study also clearly highlights the utility and clinical relevance of comprehensive genomic profiling in the diagnostic workflow of histiocytic neoplasms.

8. REFERENCES

1. Siegel RL, Giaquinto AN, Jemal A. Cancer statistics, 2024. CA Cancer J Clin. 2024;74(1):12-49.
2. Garami M SD, Jakab Z. Importance of the National Childhood Cancer Registry in the field of paediatric oncology care. Orv Hetil. 2014;155:732-9.
3. Alnughmush A, Fakih RE, Mohammed S, Aljurf M. Pediatric-type follicular lymphoma: a short review. Int J Hematol Oncol. 2022;11(4):IJH41.
4. Lee J, Han JH, Lee CH, Park HS, Min SK, Lee H, et al. Comparison of histological and molecular features of pediatric-type follicular lymphoma and pediatric nodal marginal zone lymphoma. Virchows Arch. 2023;482(5):849-58.
5. Koo M, Ohgami RS. Pediatric-type Follicular Lymphoma and Pediatric Nodal Marginal Zone Lymphoma: Recent Clinical, Morphologic, Immunophenotypic, and Genetic Insights. Adv Anat Pathol. 2017;24(3):128-35.
6. Demir HA, Bayhan T, Uner A, Kurtulan O, Karakus E, Emir S, et al. Chronic lymphocytic leukemia in a child: a challenging diagnosis in pediatric oncology practice. Pediatr Blood Cancer. 2014;61(5):933-5.
7. Swerdlow SH, Campo E, Harris NL, Jaffe ES, Pileri SA, Stein H, et al. WHO Classification of Tumours of Haematopoietic and Lymphoid Tissues. 4th ed. Bosman FT, Jaffe ES, Lakhani SR, Ohgaki H, editors: International Agency for Research on Cancer; 2017. 189-213 p.
8. Hunger SP, Mullighan CG. Acute Lymphoblastic Leukemia in Children. The New England journal of medicine. 2015;373(16):1541-52.
9. Greaves M. Darwin and evolutionary tales in leukemia. The Ham-Wasserman Lecture. Hematology Am Soc Hematol Educ Program. 2009:3-12.
10. Bateman CM, Alpar D, Ford AM, Colman SM, Wren D, Morgan M, et al. Evolutionary trajectories of hyperdiploid ALL in monozygotic twins. Leukemia. 2015;29(1):58-65.
11. Ma Y, Dobbins SE, Sherborne AL, Chubb D, Galbiati M, Cazzaniga G, et al. Developmental timing of mutations revealed by whole-genome sequencing of twins with acute lymphoblastic leukemia. Proc Natl Acad Sci U S A. 2013;110(18):7429-33.
12. Brady SW, Roberts KG, Gu Z, Shi L, Pounds S, Pei D, et al. The genomic landscape of pediatric acute lymphoblastic leukemia. Nat Genet. 2022;54(9):1376-89.

13. Cree IA. The WHO Classification of Haematolymphoid Tumours. Leukemia. 2022;36(7):1701-2.
14. Alaggio R, Amador C, Anagnostopoulos I, Attygalle AD, Araujo IBO, Berti E, et al. The 5th edition of the World Health Organization Classification of Haematolymphoid Tumours: Lymphoid Neoplasms. Leukemia. 2022;36(7):1720-48.
15. Aumann S, Shaulov A, Haran A, Gross Even-Zohar N, Vainstein V, Nachmias B. The Emerging Role of Venetoclax-Based Treatments in Acute Lymphoblastic Leukemia. Int J Mol Sci. 2022;23(18).
16. Mouttet B, Vinti L, Ancliff P, Bodmer N, Brethon B, Cario G, et al. Durable remissions in TCF3-HLF positive acute lymphoblastic leukemia with blinatumomab and stem cell transplantation. Haematologica. 2019;104(6):e244-e7.
17. Bobeff K, Pastorczak A, Urbanska Z, Balwierz W, Juraszewska E, Wachowiak J, et al. Venetoclax Use in Paediatric Haemato-Oncology Centres in Poland: A 2022 Survey. Children (Basel). 2023;10(4).
18. Lilljebjorn H, Henningsson R, Hyrenius-Wittsten A, Olsson L, Orsmark-Pietras C, von Palffy S, et al. Identification of ETV6-RUNX1-like and DUX4-rearranged subtypes in paediatric B-cell precursor acute lymphoblastic leukaemia. Nat Commun. 2016;7:11790.
19. Gu Z, Churchman ML, Roberts KG, Moore I, Zhou X, Nakitandwe J, et al. PAX5-driven subtypes of B-progenitor acute lymphoblastic leukemia. Nat Genet. 2019;51(2):296-307.
20. Zaliova M, Winkowska L, Stuchly J, Fiser K, Triska P, Zwyrtkova M, et al. A novel class of ZNF384 aberrations in acute leukemia. Blood Adv. 2021;5(21):4393-7.
21. Mullighan CG, Goorha S, Radtke I, Miller CB, Coustan-Smith E, Dalton JD, et al. Genome-wide analysis of genetic alterations in acute lymphoblastic leukaemia. Nature. 2007;446(7137):758-64.
22. Mullighan CG, Phillips LA, Su X, Ma J, Miller CB, Shurtleff SA, et al. Genomic analysis of the clonal origins of relapsed acute lymphoblastic leukemia. Science. 2008;322(5906):1377-80.
23. Iacobucci I, Mullighan CG. Genetic Basis of Acute Lymphoblastic Leukemia. J Clin Oncol. 2017;35(9):975-83.

24. Forero-Castro M, Robledo C, Benito R, Abaigar M, Africa Martin A, Arefi M, et al. Genome-Wide DNA Copy Number Analysis of Acute Lymphoblastic Leukemia Identifies New Genetic Markers Associated with Clinical Outcome. PLoS One. 2016;11(2):e0148972.

25. Paulsson K, Johansson B. High hyperdiploid childhood acute lymphoblastic leukemia. Genes Chromosomes Cancer. 2009;48(8):637-60.

26. Paulsson K, Lilljebjörn H, Biloglav A, Olsson L, Rissler M, Castor A, et al. The genomic landscape of high hyperdiploid childhood acute lymphoblastic leukemia. Nat Genet. 2015;47(6):672-6.

27. Pajor L, Szuhai K, Mehes G, Kosztolanyi G, Jakso P, Lendvai G, et al. Combined metaphase, interphase cytogenetic, and flow cytometric analysis of DNA content of pediatric acute lymphoblastic leukemia. Cytometry. 1998;34(2):87-94.

28. Schwab CJ, Jones LR, Morrison H, Ryan SL, Yigittop H, Schouten JP, et al. Evaluation of multiplex ligation-dependent probe amplification as a method for the detection of copy number abnormalities in B-cell precursor acute lymphoblastic leukemia. Genes Chromosomes Cancer. 2010;49(12):1104-13.

29. Alpar D, de Jong D, Savola S, Yigittop H, Kajtar B, Kereskai L, et al. MLPA is a powerful tool for detecting lymphoblastic transformation in chronic myeloid leukemia and revealing the clonal origin of relapse in pediatric acute lymphoblastic leukemia. Cancer Genet. 2012;205(9):465-9.

30. Benard-Slagter A, Zondervan I, de Groot K, Ghazavi F, Sarhadi V, Van Vlierberghe P, et al. Digital Multiplex Ligation-Dependent Probe Amplification for Detection of Key Copy Number Alterations in T- and B-Cell Lymphoblastic Leukemia. J Mol Diagn. 2017;19(5):659-72.

31. Thakral D, Kaur G, Gupta R, Benard-Slagter A, Savola S, Kumar I, et al. Rapid Identification of Key Copy Number Alterations in B- and T-Cell Acute Lymphoblastic Leukemia by Digital Multiplex Ligation-Dependent Probe Amplification. Front Oncol. 2019;9:871.

32. Kiss R, Gango A, Benard-Slagter A, Egyed B, Haltrich I, Hegyi L, et al. Comprehensive profiling of disease-relevant copy number aberrations for advanced clinical diagnostics of pediatric acute lymphoblastic leukemia. Mod Pathol. 2020;33(5):812-24.

33. Raimondi SC, Pui CH, Hancock ML, Behm FG, Filatov L, Rivera GK. Heterogeneity of hyperdiploid (51-67) childhood acute lymphoblastic leukemia. Leukemia. 1996;10(2):213-24.
34. Heerema NA, Sather HN, Sensel MG, Zhang T, Hutchinson RJ, Nachman JB, et al. Prognostic impact of trisomies of chromosomes 10, 17, and 5 among children with acute lymphoblastic leukemia and high hyperdiploidy (> 50 chromosomes). J Clin Oncol. 2000;18(9):1876-87.
35. Moorman AV, Richards SM, Martineau M, Cheung KL, Robinson HM, Jalali GR, et al. Outcome heterogeneity in childhood high-hyperdiploid acute lymphoblastic leukemia. Blood. 2003;102(8):2756-62.
36. Dastugue N, Suciu S, Plat G, Speleman F, Cave H, Girard S, et al. Hyperdiploidy with 58-66 chromosomes in childhood B-acute lymphoblastic leukemia is highly curable: 58951 CLG-EORTC results. Blood. 2013;121(13):2415-23.
37. Harris RL, Harrison CJ, Martineau M, Taylor KE, Moorman AV. Is trisomy 5 a distinct cytogenetic subgroup in acute lymphoblastic leukemia? Cancer Genet Cytogenet. 2004;148(2):159-62.
38. Vojcek A, Pajor G, Alpar D, Matics R, Poto L, Szuhai K, et al. Conserved hierarchical gain of chromosome 4 is an independent prognostic factor in high hyperdiploid pediatric acute lymphoblastic leukemia. Leuk Res. 2017;52:28-33.
39. Harris MB, Shuster JJ, Carroll A, Look AT, Borowitz MJ, Crist WM, et al. Trisomy of leukemic cell chromosomes 4 and 10 identifies children with B-progenitor cell acute lymphoblastic leukemia with a very low risk of treatment failure: a Pediatric Oncology Group study. Blood. 1992;79(12):3316-24.
40. Sutcliffe MJ, Shuster JJ, Sather HN, Camitta BM, Pullen J, Schultz KR, et al. High concordance from independent studies by the Children's Cancer Group (CCG) and Pediatric Oncology Group (POG) associating favorable prognosis with combined trisomies 4, 10, and 17 in children with NCI Standard-Risk B-precursor Acute Lymphoblastic Leukemia: a Children's Oncology Group (COG) initiative. Leukemia. 2005;19(5):734-40.
41. Enshaei A, Vora A, Harrison CJ, Moppett J, Moorman AV. Defining low-risk high hyperdiploidy in patients with paediatric acute lymphoblastic leukaemia: a

retrospective analysis of data from the UKALL97/99 and UKALL2003 clinical trials. Lancet Haematol. 2021;8(11):e828-e39.

42. Mullighan CG, Su X, Zhang J, Radtke I, Phillips LA, Miller CB, et al. Deletion of IKZF1 and prognosis in acute lymphoblastic leukemia. The New England journal of medicine. 2009;360(5):470-80.

43. Harrison CJ, Moorman AV, Schwab C, Carroll AJ, Raetz EA, Devidas M, et al. An international study of intrachromosomal amplification of chromosome 21 (iAMP21): cytogenetic characterization and outcome. Leukemia. 2014;28(5):1015-21.

44. Stanulla M, Dagdan E, Zaliova M, Moricke A, Palmi C, Cazzaniga G, et al. IKZF1(plus) Defines a New Minimal Residual Disease-Dependent Very-Poor Prognostic Profile in Pediatric B-Cell Precursor Acute Lymphoblastic Leukemia. J Clin Oncol. 2018;36(12):1240-9.

45. Moorman AV, Enshaei A, Schwab C, Wade R, Chilton L, Elliott A, et al. A novel integrated cytogenetic and genomic classification refines risk stratification in pediatric acute lymphoblastic leukemia. Blood. 2014;124(9):1434-44.

46. Hamadeh L, Enshaei A, Schwab C, Alonso CN, Attarbaschi A, Barbany G, et al. Validation of the United Kingdom copy-number alteration classifier in 3239 children with B-cell precursor ALL. Blood Adv. 2019;3(2):148-57.

47. Khoury JD, Solary E, Abla O, Akkari Y, Alaggio R, Apperley JF, et al. The 5th edition of the World Health Organization Classification of Haematolymphoid Tumours: Myeloid and Histiocytic/Dendritic Neoplasms. Leukemia. 2022;36(7):1703-19.

48. Emile JF, Abla O, Fraitag S, Horne A, Haroche J, Donadieu J, et al. Revised classification of histiocytoses and neoplasms of the macrophage-dendritic cell lineages. Blood. 2016;127(22):2672-81.

49. Chan JK, Lamant L, Algar E, Delsol G, Tsang WY, Lee KC, et al. ALK+ histiocytosis: a novel type of systemic histiocytic proliferative disorder of early infancy. Blood. 2008;112(7):2965-8.

50. Lucas CG, Gilani A, Solomon DA, Liang X, Maher OM, Chamyan G, et al. ALK-positive histiocytosis with KIF5B-ALK fusion in the central nervous system. Acta Neuropathol. 2019;138(2):335-7.

51. Jaffe ES, Chan JKC. Histiocytoses converge through common pathways. Blood. 2022;139(2):157-9.

52. Kemps PG, Picarsic J, Durham BH, Helias-Rodzewicz Z, Hiemcke-Jiwa L, van den Bos C, et al. ALK-positive histiocytosis: a new clinicopathologic spectrum highlighting neurologic involvement and responses to ALK inhibition. Blood. 2022;139(2):256-80.
53. McClain KL, Bigenwald C, Collin M, Haroche J, Marsh RA, Merad M, et al. Histiocytic disorders. Nat Rev Dis Primers. 2021;7(1):73.
54. Emile JF, Cohen-Aubart F, Collin M, Fraitag S, Idbaih A, Abdel-Wahab O, et al. Histiocytosis. Lancet. 2021;398(10295):157-70.
55. Salama HA, Jazieh AR, Alhejazi AY, Absi A, Alshieban S, Alzahrani M, et al. Highlights of the Management of Adult Histiocytic Disorders: Langerhans Cell Histiocytosis, Erdheim-Chester Disease, Rosai-Dorfman Disease, and Hemophagocytic Lymphohistiocytosis. Clin Lymphoma Myeloma Leuk. 2021;21(1):e66-e75.
56. Diamond EL, Durham BH, Ulaner GA, Drill E, Buthorn J, Ki M, et al. Efficacy of MEK inhibition in patients with histiocytic neoplasms. Nature. 2019;567(7749):521-4.
57. Swerdlow SH, Campo E, Pileri SA, Harris NL, Stein H, Siebert R, et al. The 2016 revision of the World Health Organization classification of lymphoid neoplasms. Blood. 2016;127(20):2375-90.
58. Swerdlow SH, Campo E, Harris NL, Jaffe ES, Pileri SA, Stein H, et al. WHO Classification of Tumours of Haematopoietic and Lymphoid Tissues. Bosman FT, Jaffe ES, Lakhani SR, Ohgaki H, editors. Lyon: International Agency for Research on Cancer; 2008. 167-78 p.
59. Stary J, Zimmermann M, Campbell M, Castillo L, Dibar E, Donska S, et al. Intensive chemotherapy for childhood acute lymphoblastic leukemia: results of the randomized intercontinental trial ALL IC-BFM 2002. J Clin Oncol. 2014;32(3):174-84.
60. Talevich E, Shain AH, Botton T, Bastian BC. CNVkit: Genome-Wide Copy Number Detection and Visualization from Targeted DNA Sequencing. PLoS Comput Biol. 2016;12(4):e1004873.
61. Olshen AB, Bengtsson H, Neuvial P, Spellman PT, Olshen RA, Seshan VE. Parent-specific copy number in paired tumor-normal studies using circular binary segmentation. Bioinformatics. 2011;27(15):2038-46.

62. Venkatraman ES, Olshen AB. A faster circular binary segmentation algorithm for the analysis of array CGH data. Bioinformatics. 2007;23(6):657-63.
63. Mayakonda A, Lin DC, Assenov Y, Plass C, Koeffler HP. Maftools: efficient and comprehensive analysis of somatic variants in cancer. Genome Res. 2018;28(11):1747-56.
64. H L. Aligning sequence reads, clone sequences and assembly contigs with BWA-MEM2013.
65. Li H, Handsaker B, Wysoker A, Fennell T, Ruan J, Homer N, et al. The Sequence Alignment/Map format and SAMtools. Bioinformatics. 2009;25(16):2078-9.
66. Paila U, Chapman BA, Kirchner R, Quinlan AR. GEMINI: integrative exploration of genetic variation and genome annotations. PLoS Comput Biol. 2013;9(7):e1003153.
67. Wang G, Dunbrack RL, Jr. PISCES: a protein sequence culling server. Bioinformatics. 2003;19(12):1589-91.
68. Chen X, Schulz-Trieglaff O, Shaw R, Barnes B, Schlesinger F, Kallberg M, et al. Manta: rapid detection of structural variants and indels for germline and cancer sequencing applications. Bioinformatics. 2016;32(8):1220-2.
69. Bedics G, Csoka M, Reiniger L, Varga E, Liptai Z, Papp G, et al. Novel actionable ROS1::GIT2 fusion in non-Langerhans cell histiocytosis with central nervous system involvement. Acta Neuropathol. 2023;145(1):153-6.
70. Mullighan CG, Miller CB, Radtke I, Phillips LA, Dalton J, Ma J, et al. BCR-ABL1 lymphoblastic leukaemia is characterized by the deletion of Ikaros. Nature. 2008;453(7191):110-4.
71. Papaemmanuil E, Rapado I, Li Y, Potter NE, Wedge DC, Tubio J, et al. RAG-mediated recombination is the predominant driver of oncogenic rearrangement in ETV6-RUNX1 acute lymphoblastic leukemia. Nat Genet. 2014;46(2):116-25.
72. Parker H, An Q, Barber K, Case M, Davies T, Konn Z, et al. The complex genomic profile of ETV6-RUNX1 positive acute lymphoblastic leukemia highlights a recurrent deletion of TBL1XR1. Genes Chromosomes Cancer. 2008;47(12):1118-25.
73. Usvasalo A, Ninomiya S, Raty R, Hollmen J, Saarinen-Pihkala UM, Elonen E, et al. Focal 9p instability in hematologic neoplasias revealed by comparative genomic hybridization and single-nucleotide polymorphism microarray analyses. Genes Chromosomes Cancer. 2010;49(4):309-18.

74. Scheijen B, Boer JM, Marke R, Tijchon E, van Ingen Schenau D, Waanders E, et al. Tumor suppressors BTG1 and IKZF1 cooperate during mouse leukemia development and increase relapse risk in B-cell precursor acute lymphoblastic leukemia patients. Haematologica. 2017;102(3):541-51.
75. Schwab CJ, Chilton L, Morrison H, Jones L, Al-Shehhi H, Erhorn A, et al. Genes commonly deleted in childhood B-cell precursor acute lymphoblastic leukemia: association with cytogenetics and clinical features. Haematologica. 2013;98(7):1081-8.
76. Stanulla M, Cavé H, Moorman AV. IKZF1 deletions in pediatric acute lymphoblastic leukemia: still a poor prognostic marker? Blood. 2020;135(4):252-60.
77. Ayon-Perez MF, Pimentel-Gutierrez HJ, Duran-Avelar MJ, Vibanco-Perez N, Perez-Peraza VM, Perez-Gonzalez OA, et al. IKZF1 Gene Deletion in Pediatric Patients Diagnosed with Acute Lymphoblastic Leukemia in Mexico. Cytogenet Genome Res. 2019;158(1):10-6.
78. van der Veer A, Waanders E, Pieters R, Willemse ME, Van Reijmersdal SV, Russell LJ, et al. Independent prognostic value of BCR-ABL1-like signature and IKZF1 deletion, but not high CRLF2 expression, in children with B-cell precursor ALL. Blood. 2013;122(15):2622-9.
79. Waanders E, van der Velden VH, van der Schoot CE, van Leeuwen FN, van Reijmersdal SV, de Haas V, et al. Integrated use of minimal residual disease classification and IKZF1 alteration status accurately predicts 79% of relapses in pediatric acute lymphoblastic leukemia. Leukemia. 2011;25(2):254-8.
80. Marke R, van Leeuwen FN, Scheijen B. The many faces of IKZF1 in B-cell precursor acute lymphoblastic leukemia. Haematologica. 2018;103(4):565-74.
81. Boer JM, van der Veer A, Rizopoulos D, Fiocco M, Sonneveld E, de Groot-Kruseman HA, et al. Prognostic value of rare IKZF1 deletion in childhood B-cell precursor acute lymphoblastic leukemia: an international collaborative study. Leukemia. 2016;30(1):32-8.
82. Felice MS, Rubio PL, Digiorge J, Barreda Frank M, Martinez CS, Guitter MR, et al. Impact of IKZF1 Deletions in the Prognosis of Childhood Acute Lymphoblastic Leukemia in Argentina. Cancers. 2022;14(13).
83. Inaba H, Mullighan CG. Pediatric acute lymphoblastic leukemia. Haematologica. 2020;105(11):2524-39.

84. Diamond EL, Durham BH, Haroche J, Yao Z, Ma J, Parikh SA, et al. Diverse and Targetable Kinase Alterations Drive Histiocytic Neoplasms. Cancer Discov. 2016;6(2):154-65.
85. Garces S, Medeiros LJ, Marques-Piubelli ML, Coelho Siqueira SA, Miranda RN, Cuglievan B, et al. Cyclin D1 expression in Rosai-Dorfman disease: a near-constant finding that is not invariably associated with mitogen-activated protein kinase/extracellular signal-regulated kinase pathway activation. Hum Pathol. 2022;121:36-45.
86. Rikova K, Guo A, Zeng Q, Possemato A, Yu J, Haack H, et al. Global survey of phosphotyrosine signaling identifies oncogenic kinases in lung cancer. Cell. 2007;131(6):1190-203.
87. Drilon A, Jenkins C, Iyer S, Schoenfeld A, Keddy C, Davare MA. ROS1-dependent cancers - biology, diagnostics and therapeutics. Nat Rev Clin Oncol. 2021;18(1):35-55.
88. Helgager J, Lidov HG, Mahadevan NR, Kieran MW, Ligon KL, Alexandrescu S. A novel GIT2-BRAF fusion in pilocytic astrocytoma. Diagn Pathol. 2017;12(1):82.
89. Walz C, Metzgeroth G, Haferlach C, Schmitt-Graeff A, Fabarius A, Hagen V, et al. Characterization of three new imatinib-responsive fusion genes in chronic myeloproliferative disorders generated by disruption of the platelet-derived growth factor receptor beta gene. Haematologica. 2007;92(2):163-9.
90. Ardini E, Siena S. Entrectinib approval by EMA reinforces options for ROS1 and tumour agnostic NTRK targeted cancer therapies. ESMO Open. 2020;5(5):e000867.

9. BIBLIOGRAPHY OF THE CANDIDATE'S PUBLICATIONS

Publications related to the PhD thesis:

1.

Bedics, Gábor ; Egyed, Bálint* ; Kotmayer, Lili ; Benard-Slagter, Anne ; de Groot, Karel ; Bekő, Anna ; Hegyi, Lajos László ; Bátai, Bence ; Krizsán, Szilvia ; Kriván, Gergely; Erdélyi, Dániel J. ; Müller, Judit; Haltrich, Irén ; Kajtár, Béla ; Pajor, László ; Vojcek, Ágnes ; Ottóffy, Gábor ; Ujfalusi, Anikó ; Szegedi, István ; Tiszlavicz, Lilla Györgyi ; Bartyik, Katalin ; Csanádi, Krisztina ; Péter, György ; Simon, Réka ; Hauser, Péter ; Kelemen, Ágnes ; Sebestyén, Endre ; Jakab, Zsuzsanna ; Matolcsy, András ; Kiss, Csongor ; Kovács, Gábor ; Savola, Suvi ; Bödör, Csaba ; Alpár, Donát
PersonALL: a genetic scoring guide for personalized risk assessment in pediatric B-cell precursor acute lymphoblastic leukemia, BRITISH JOURNAL OF CANCER, 129 : 3 pp. 455-465. , 11 p. (2023), * joint first author

2.

Bedics, Gábor ; Csóka, Monika* ; Reiniger, Lilla ; Varga, Edit ; Liptai, Zoltán ; Papp, Gergő ; Bekő, Anna ; Cervi, Catherine ; Bödör, Csaba ; Scheich, Bálint
Novel actionable ROS1::GIT2 fusion in non-Langerhans cell histiocytosis with central nervous system involvement, ACTA NEUROPATHOLOGICA 145 : 1 pp. 153-156. , 4 p. (2023), * joint first author

Other publications:

1.

Bedics, Gábor ; Kotmayer, Lili ; Zajta, Erik ; Hegyi, Lajos László ; Brückner, Edit Ágota ; Rajnai, Hajnalka ; Reiniger, Lilla ; Bödör, Csaba ; Garami, Miklós ; Scheich, Bálint
Germline MUTYH mutations and high-grade gliomas: Novel evidence for a potential association, GENES CHROMOSOMES & CANCER 61 : 10 pp. 622-628. , 7 p. (2022)

2.

Bedics, Gábor ; Szőke, Péter ; Bátai, Bence ; Nagy, Tibor ; Papp, Gergő ; Kránitz, Noémi ; Rajnai, Hajnalka ; Reiniger, Lilla ; Bödör, Csaba ; Scheich, Bálint
Novel, clinically relevant genomic patterns identified by comprehensive genomic profiling in ATRX-deficient IDH-wildtype adult high-grade gliomas, SCIENTIFIC REPORTS 13 : 1 Paper: 18436 , 12 p. (2023)

3.

Jia, Xinkai ; Gábris, Fanni ; Jacobsen, Óli ; **Bedics, Gábor** ; Botz, Bálint ; Helyes, Zsuzsanna ; Kellermayer, Zoltán ; Vojkovics, Dóra ; Berta, Gergely ; Nagy, Nándor ; Jakus, Zoltán ; Balogh, Péter
Foliate Lymphoid Aggregates as Novel Forms of Serous Lymphocyte Entry Sites of Peritoneal B Cells and High-Grade B Cell Lymphomas, JOURNAL OF IMMUNOLOGY 204 : 1 pp. 23-36. , 14 p. (2020)

4.

Kellermayer, Dalma ; Tordai, Hedvig ; Kiss, Balázs ; Török, György ; Péter, Dániel M. ; Sayour, Alex Ali ; Pólos, Miklós ; Hartyánszky, István ; Szilveszter, Bálint ; Labeit, Siegfried; Gángó, Ambrus ; **Bedics, Gábor** ; Bödör, Csaba ; Radovits, Tamás ; Merkely, Béla ; Kellermayer, Miklós S.Z.
Truncated titin is structurally integrated into the human dilated cardiomyopathic sarcomere, JOURNAL OF CLINICAL INVESTIGATION 134 : 2 Paper: e169753 , 13 p. (2024)

5.

Jenei, Alex ; **Bedics, Gábor** ; Erdélyi, Dániel J. ; Müller, Judit ; Györke, Tamás ; Bödör, Csaba ; Szepesi, Ágota

Potential role of MAP2K1 mutation in the trans-differentiation of interdigitating dendritic cell sarcoma: Case report and literature review, FRONTIERS IN PEDIATRICS 10 Paper: 959307 , 6 p. (2022)

6.

Krizsán, Szilvia ; Péterffy, Borbála ; Egyed, Bálint ; Nagy, Tibor ; Sebestyén, Endre ; Hegyi, Lajos László ; Jakab, Zsuzsanna ; Erdélyi, Dániel J. ; Müller, Judit ; Péter, György ; Csanádi, Krisztina; Kállay, Krisztián ; Kriván, Gergely ; Barna, Gábor ; **Bedics, Gábor** ; Haltrich, Irén ; Ottóffy, Gábor ; Csernus, Katalin ; Vojcek, Ágnes ; Tiszlavicz, Lilla Györgyi ; Gábor, Krisztina Mita ; Kelemen, Ágnes ; Hauser, Péter ; Gaál, Zsuzsanna ; Szegedi, István ; Ujfalusi, Anikó ; Kajtár, Béla ; Kiss, Csongor ; Matolcsy, András ; Tímár, Botond ; Kovács, Gábor ; Alpár, Donát ; Bödör, Csaba

Next-generation sequencing-based genomic profiling of children diagnosed with acute myeloid leukemia, JOURNAL OF MOLECULAR DIAGNOSTICS 25 : 8 pp. 555-568. , 14 p. (2023)

7.

Váradi, Melinda ; Nagy, Nikolett ; Reis, Henning ; Hadaschik, Boris ; Niedworok, Christian ; Módos, Orsolya ; Szendrői, Attila ; Ablat, Jason ; Black, Peter C. ; Keresztes, Dávid ; Csizmarik, Anita ; Olah, Csilla ; Gaisa, Nadine T. ; Kiss, András ; Timár, József ; Tóth, Erika ; Csernak, Erzsebet ; Gerstner, Árpád ; Mittal, Vinay ; Karkampouna, Sofia ; Kruithof de Julio, Marianna ; Győrffy, Balázs ; **Bedics, Gábor** ; Rink, Michael ; Fisch, Margit ; Nyirády, Péter ; Szarvas, Tibor

Clinical sequencing identifies potential actionable alterations in a high rate of urachal and primary bladder adenocarcinomas, CANCER MEDICINE 12 : 7 pp. 9041-9054. , 14 p. (2023)

8.

Sztankovics, Dániel ; Krencz, Ildikó ; Moldvai, Dorottya ; Dankó, Titanilla ; Nagy, Ákos ; Nagy, Noémi ; **Bedics, Gábor** ; Rókusz, András ; Papp, Gergő ; Tőkés, Anna-Mária ; Pápay, Judit ; Sápi, Zoltán ; Dezső, Katalin ; Bödör, Csaba ; Sebestyén, Anna
Novel RICTOR amplification harbouring entities: FISH validation of RICTOR amplification in tumour tissue after next-generation sequencing, SCIENTIFIC REPORTS 13 : 1 Paper: 19610 , 12 p. (2023)

9.

Cervi, Catherine ; Sápi, Zoltán ; **Bedics, Gábor** ; Zajta, Erik ; Hegyi, Lajos ; Pápay, Judit ; Dezső, Katalin ; Varga, Edit ; Mudra, Katalin ; Bödör, Csaba ; Csóka, Monika
Case report: Complete and durable response to larotrectinib (TRK inhibitor) in an infant diagnosed with angiosarcoma harbouring a KHDRBS1-NTRK3 fusion gene, FRONTIERS IN ONCOLOGY 13 Paper: 999810 , 6 p. (2023)

10.

Stark, Júlia ; Tőke, Judit ; Huszty, Gergely ; Nagy, Péter ; **Bedics, Gábor** ; Bödör, Csaba ; Tímár, József ; Tóth, Miklós
Parathyroid cancer with MTOR gene mutation: Case report and review of the literature, ANNALES D ENDOCRINOLOGIE 84 : 6 pp. 761-763. , 3 p. (2023)

11.

Lippai, Zoltán ; Péterfia, Bálint ; Papp, Gergő ; Dezső, Katalin ; Bedics, Gábor ; Pápai, Zsuzsanna ; Lamers, Meindert H. ; Kuin, Rosan CM ; Szuhai, Károly** ; Sápi, Zoltán
A recurrent NTRK1 tyrosine kinase domain mutation pair is characteristic in a subset of dedifferentiated liposarcomas, EUROPEAN JOURNAL OF CANCER 202 Paper: 114005 , 9 p. (2024)

12.

Bedics, Gábor ; Sebestyén, Endre
[*Basic concepts of diagnostic application of next-generation sequencing – a practical introduction to precision medicine*], ORVOSKÉPZÉS 96 : 3 pp. 343-355. , 13 p. (2021), (Hungarian)

13.

Brückner, Edit ; **Bedics, Gábor** ; Reiniger, Lilla ; Rajnai, Hajnalka ; Jakab, Zsuzsanna ; Bödör, Csaba ; Scheich, Bálint ; Garami, Miklós

[*Childhood brain tumors: diagnosis and therapy - comprehensive genomic profiling*], MAGYAR ONKOLÓGIA 67 : 4 pp. 315-320. , 6 p. (2023), (Hungarian)

14.

Szabó, Sándor ; **Bedics, Gábor** ; Bödör, Csaba ; Csóka, Monika

[*Tumor agnostic therapy in pediatric oncology*], KLINIKAI ONKOLÓGIA 10 : 2 pp. 127-132. , 6 p. (2023), (Hungarian)

15.

Brückner, Edit ; **Bedics, Gábor** ; Rajnai, Hajnalka ; Bödör, Csaba ; Garami, Miklós

[*The role of comprehensive genomic profiling in the design of therapy for childhood brain tumours*], GYERMEKGYÓGYÁSZAT 72 : 6 pp. 429-434. , 6 p. (2021), (Hungarian)

10. ACKNOWLEDGEMENTS

I am grateful to András Matolcsy, MD, PhD, DSc, Head of the Department of Pathology and Experimental Cancer Research at Semmelweis University, for allowing me to pursue PhD studies in the host Institute.

I would like to thank my supervisor, Donát Alpár, PhD for his many highly valuable pieces of advice and his accurate attitude, which example served me as a guide during my PhD studies.

I would like to express my sincere gratitude to my mentor and Head of the Molecular Oncohematology Research Group, Csaba Bödör, PhD, DSc, for the tremendous support he provided me and for the friendly ambiance, he created in our laboratory.

I am grateful to Bálint Scheich, MD, PhD, for the fruitful collaboration projects and for teaching me how to be alerted for discovering very exciting novelties during diagnostic histopathological analyses.

I am grateful to Endre Sebestyén PhD, for the high-quality bioinformatics training he provided me.

I am grateful to Lili Kotmayer MD, PhD for her friendship, which provided me a day-to-day support to overcome obstacles, and have better insights to other fields of molecular oncohematology.

I would like to thank Bence Bátai MD, a close colleague and friend of mine for his companionship in bioinformatic training and problem-solving, and for sharing some pieces of his deep clinical knowledge in hematology with me.

I wish to thank all the colleagues and members of the HCEMM-SE Molecular Oncohematology Research Group for creating a friendly and inspiring work environment

I could benefit from every day. I also owe thanks to every employee of the Institute for their great support.

I owe the greatest thanks to my family: to my dear wife and children for their support and love during my PhD studies.

The research studies were funded by the Hungarian National Research, Development and Innovation Office (NKFIH) (FK20_134253, K21_137948 and K22_143021), the EU's Horizon 2020 research and innovation program (No. 739593), the Hungarian Pediatric Oncology Network, the Co-operative Doctoral Program of the Ministry for Innovation and Technology (KDP-2020-1008491), the János Bolyai Research Scholarship program (ID: BO/00125/22) of the Hungarian Academy of Sciences, as well as by the Complementary Research Excellence Program of Semmelweis University (EFOP-3.6.3-VEKOP-16-2017-00009), the Ministry of Innovation and Technology of Hungary from the New National Excellence Program (ÚNKP-22-5-SE-7 and ÚNKP-22–3-II) and the National Research, Development and Innovation Fund, financed under the TKP2021-EGA-24, TKP2021-NVA-11 and TKP2021-NVA-15 funding schemes and the ELIXIR Hungary. Open access fundings were provided by Semmelweis University.